

Spatial Weather, Socio-Economic and Political Risks in Probabilistic Load Forecasting

Monika Zimmermann^{a,*}, Florian Ziel^a

^a*Chair of Environmental Economics, esp. Economics of Renewable Energy
University of Duisburg-Essen
Germany*

Abstract

Accurate forecasts of the impact of spatial weather and pan-European socio-economic and political risks on hourly electricity demand for the mid-term horizon are crucial for strategic decision-making amidst the inherent uncertainty. Most importantly, these forecasts are essential for the operational management of power plants, ensuring supply security and grid stability, and in guiding energy trading and investment decisions. The primary challenge for this forecasting task lies in disentangling the multifaceted drivers of load, which include national deterministic (daily, weekly, annual, and holiday patterns) and national stochastic weather and autoregressive effects. Additionally, transnational stochastic socio-economic and political effects add further complexity, in particular, due to their non-stationarity. To address this challenge, we present an interpretable probabilistic mid-term forecasting model for the hourly load that captures, besides all deterministic effects, the various uncertainties in load. This model recognizes transnational dependencies across 24 European countries, with multivariate modeled socio-economic and political states and cross-country dependent forecasting. Built from interpretable Generalized Additive Models (GAMs), the model enables an analysis of the transmission of each incorporated effect to the hour-specific load. Our findings highlight the vulnerability of countries reliant on electric heating under extreme weather scenarios. This emphasizes the need for high-resolution forecasting of weather effects on pan-European electricity consumption especially in anticipation of widespread electric heating adoption.

Keywords: Electricity Demand, Generalized Additive Models, Geopolitical Risk, High-resolution modeling, Temperature Risk, Trend Behavior

1. Introduction

While weather, socio-economic and political risks are well-discussed for the security of gas supplies, see e.g [Goodell et al. \(2023\)](#); [Shen et al. \(2023\)](#), their impact on the security of electricity load remains mostly overlooked. This is particularly concerning as Europe rapidly transitions from gas heating to electric heat pumps. This transition, driven by decarbonization goals and the desire for long-term independence from unreliable gas suppliers, especially since the Russian invasion of Ukraine, see e.g. [Altermatt et al. \(2023\)](#); [Roth et al. \(2023\)](#), introduces similar risks for load security. By way of illustration, pan-European and single-country scenario analyses predict doubling or even higher increases in electricity demand to

*Corresponding author

Email addresses: [Monika.Zimmermann](mailto:Monika.Zimmermann@uni-due.de), [Florian.Ziel](mailto:Florian.Ziel@uni-due.de)

accommodate heat pump requirements, even in moderate scenarios where only 25% of building heating is electrified, see Kröger et al. (2023); Roth (2023); Watson et al. (2023); Staffell & Pfenninger (2018). Additionally, Bogdanov et al. (2024); Ruhnau et al. (2023) emphasize the dependence of heat pump performance on temperature, further amplifying weather-related risks to electricity load. Combined with policymakers' incentives to decarbonize not only heating but also transportation across Europe and the increasing interconnection of European power grids, these factors introduce significant cross-country dependent uncertainty into future load modeling.

As a result, forecasting the impact of uncertain weather, socio-economic and political scenarios on electricity load jointly across Europe is becoming increasingly essential to ensure supply security and grid stability, and to guide energy trading and investment decisions. Considering the time frame of the influence of these risks, such forecasts are needed for the mid-term horizon (several weeks to one year). Additionally, due to the dynamics of the electricity market and resulting power grid management, these forecasts require an hourly resolution, as argued by González Grandón et al. (2024); Behm et al. (2020); Agrawal et al. (2018); Hong et al. (2014).

The primary challenge for this forecasting task lies in the decomposition of the various deterministic and uncertain effects on load, their varying spatial level and cross-country dependence. Following Pierrot & Goude (2011), the factors impacting load can be categorized into four main groups: Firstly, load is influenced by deterministic calendar effects. These country-specific effects encompass the calendar-based behavior of a country's society (daily, weekly, annual, and holiday patterns). Secondly, load is affected by stochastic weather effects. While weather primarily affects load at the national level, reflecting its regional formation, underlying weather conditions influence transnational load. Thirdly, stochastic socio-economic and political effects influence load in their non-stationarity trend behavior. With strong cross-country dependencies in economic well-being and an increasing legislative power of the European Parliament, these effects are transnational. Examples include load effects due to recent crises like COVID-19 and the Russian invasion of Ukraine. Lastly, remaining stochastic and primarily national autoregressive terms affect load.

Existing load forecasting research primarily focuses on short-term horizons (hours to a few days), typically at the country level or with even finer spatial granularity, as reviewed by Verwiebe et al. (2021) and Davis et al. (2016). Models with an hourly resolution for the mid-term horizon and multivariate approaches capturing cross-country dependencies remain scarce. While some studies have incorporated weather uncertainty into probabilistic load forecasting, see Ludwig et al. (2023); Dordonnat et al. (2016), to the best of our knowledge, no existing model assesses a cross-country dependent combined impact of socio-economic and political risks alongside weather risk on electricity load.

Methods that are applied in probabilistic load forecasting are wide-ranging, from classical quantile, density and trajectory ensembling forecasting, see e.g. Haben et al. (2023) for a concise overview, to sophisticated machine learning models based on e.g. different types of neural networks, gaussian process models or quantile regression forest, see e.g. Wang et al. (2024); Yang et al. (2024); Baviera & Messuti (2023); Li et al. (2023); Zhang et al. (2023); Brusaferri et al. (2022). Recent advancements encompass hybrid models combining diverse forecasting methods, as summarized by Petropoulos et al. (2022) and

Hong et al. (2016). Examples include studies by De Vilmaest et al. (2024); Lu et al. (2023); Dudek (2022) that utilized among others combinations with Generalized Additive Models (GAMs).

Building upon early GAM-based methods in load forecasting, see e.g. Pierrot & Goude (2011); Fan & Hyndman (2012); Goude et al. (2014), the effectiveness of GAMs in probabilistic load forecasting is now well-established. For instance, winning methods in the IEEE DataPort Competition by De Vilmaest & Goude (2022) employed GAMs within model ensembles. Similarly, GAMs consistently ranked highly in previous forecasting competitions, securing top positions in GEFCOM 2014 Hong et al. (2016), see Gaillard et al. (2016); Dordonnat et al. (2016).

By applying linear model structures to non-linear functions along with discretization techniques, GAMs remain interpretable and efficient in estimation while capturing non-linear relationships Lepore et al. (2022); Wood (2006). Motivated by this combination of attributes and the success of GAMs in both forecasting competitions and recent research on probabilistic load forecasting, see e.g. Gilbert et al. (2023); Browell & Fasiolo (2021), we adopted this framework as the foundation for our proposed model.

Specifically, our hourly mid-term forecasting approach combines interpretable GAMs in smoothed temperatures, non-stationary socio-economic and political state variables and calendar effects, with autoregressive post-processing. It addresses uncertainties in load forecasting by trajectory ensembling from probabilistic temperature, socio-economic and political state, and autoregressive forecasts that incorporate cross-country dependencies. Our model simultaneously accounts for country-specific characteristics in load by modeling the effect of each model input individually at the country level. With our approach, we contribute five key innovations to the field of probabilistic mid-term high-resolution load forecasting:

- (i) **High-Resolution Interpretable Model:** We develop a GAM-based probabilistic forecasting model with a comprehensive set of stochastic and deterministic load drivers as inputs. This model is interpretable in each input variable and allows us to analyze the hourly and gigawatt-level impact of individual risk factors across various plausible risk scenarios. This fine-resolution analysis provides valuable insights into the uncertainty associated with mid-term load forecasting and risk assessments in load supply security.
- (ii) **Nuanced Modelling of Transnational Interdependencies:** We employ a nuanced multivariate model that accounts for both country-specific load characteristics, such as seasonal and holiday patterns along temperature sensitivity, and pan-European commonalities, such as underlying weather or socio-economic and political conditions.
- (iii) **Unit-Root Socio-Economic and Political Effects:** To capture the gradual change in mid-term load levels driven by socio-economic and political factors, our model integrates multivariate modeled aggregate economic state variables with persistent trend behavior, specifically a unit root, and compares these to modeling approaches without a unit root assumption.
- (iv) **Comprehensive Robustness Check:** The robustness of our multivariate model in terms of accuracy and calibration is demonstrated through an extensive evaluation study incorporating 24

European countries¹, illustrated by Figure 1, for more than 9 years (2015-2024) including volatile periods due to the COVID-19 pandemic and the energy crisis caused by the Russian invasion of Ukraine.

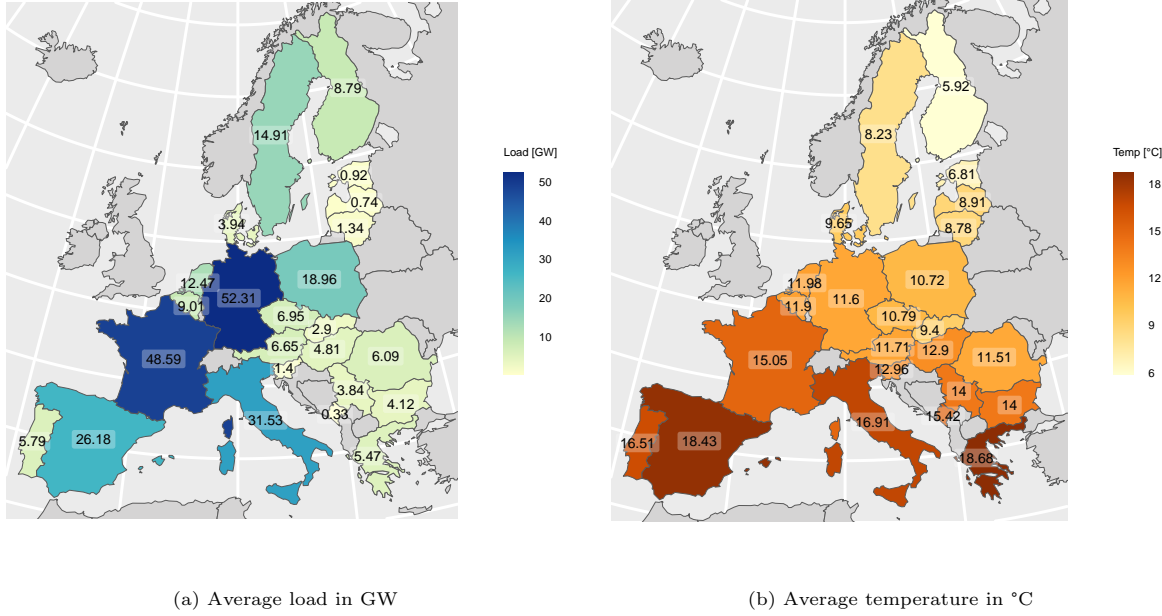


Figure 1: Average load and temperature of 2023 in the 24 European countries considered in the study.

The remainder of this paper is organized as follows: Section 2 details the multifaceted deterministic and stochastic effects on load. Section 3 introduces the applied statistical models, with a concise theoretical background on GAMs and probabilistic vector autoregressive and state models in 3.1 and 3.2, respectively. Section 4 begins with a conceptual overview of our model in 4.1 and details our modeling, estimation and forecasting specifications in 4.2. The forecasting study and evaluation design are explained in Section 5. The results of the comprehensive forecasting study are discussed and interpreted in Section 6. Finally, Section 7 concludes and outlines further research to be built upon this work. For an elaborate explanation of the corresponding point forecasting model, we refer to [Zimmermann & Ziel \(2024\)](#).

2. Deterministic and Stochastic Effects on Load

Adapting a classification proposed by [Pierrot & Goude \(2011\)](#), the various facets explaining load can be consolidated into four main groups:

- (i) **Deterministic Calender Effects:** These encompass the calender-based behavior of modern western societies entailing repetitive patterns of different seasonalities in electricity load, e.g. yearly patterns (higher load levels during winter vs. lower load levels during summer), weekly patterns

¹While data from all European countries participating in ENTSOE was initially collected, some countries were ultimately excluded from the analysis due to data quality issues.

Load Effect	Spatial Level	Type of Uncertainty
calendar	national	deterministic
weather	national-(transnational)	stochastic (multiple seasonalities)
socio-economic and political	(national)- transnational	stochastic (non-stationary with unit root)
autoregressive	national-(transnational)	stochastic

Table 1: The various facets explaining load categorized in terms of their spatial level, and type of uncertainty.

(higher load levels on weekdays vs. lower load levels on weekends), and daily patterns (higher load during the day vs. lower load during the night) and holiday patterns.

- (ii) **Stochastic Weather Effects:** These include air temperature, humidity, cloud cover, wind speed and climate change that affect load due to their impact on electric heating, cooling and lighting.
- (iii) **Stochastic Socio-Economic and Political Effects:** These involve macroeconomic, socioeconomic and energy variables along with political incentives, e.g. economic growth, population size, fossil fuel prices through industrial production or government subsidies for decarbonization, which influence, in particular in their transnational unit root behavior, mid to long-term (several months to years) levels of load.
- (iv) **Stochastic Autoregressive Effects:** These include remaining short to mid-term (hours to several weeks) autoregressive deviations in load time series.

In the subsequent sections, these drivers of load are illustrated through graphical analyses for Germany and France. These countries were chosen due to their outstanding electricity demand compared to other European countries (see Fig. 1). Additionally, France already exhibits a high dependence of load on temperature, providing initial insights into the potential impact of weather risk on load.

The load data used in the subsequent were retrieved from ENTSOE, cover the period from January 1st, 2015 to February 17th, 2024 and are available for 24 considered² in an hourly resolution. Hourly temperature observations are collected for each considered country from meteostat.net ([Meteostat Developers \(2024\)](#)) starting from January 1st, 1994, to February 17th, 2024, at weather stations located in the 5 most populous cities within each country. Holiday information was collected from Nager.Date, see [Hager \(2024\)](#), is available from January 1st to December 31st of 2000 to 2030 and encompasses both the label and the day of occurrence of the holiday. Calendar and time information, including daily, weekly, and annual seasonalities, changes due to daylight saving time and leap years are incorporated implicitly in the load time series. In all time series we adjust for daylight saving time changes.

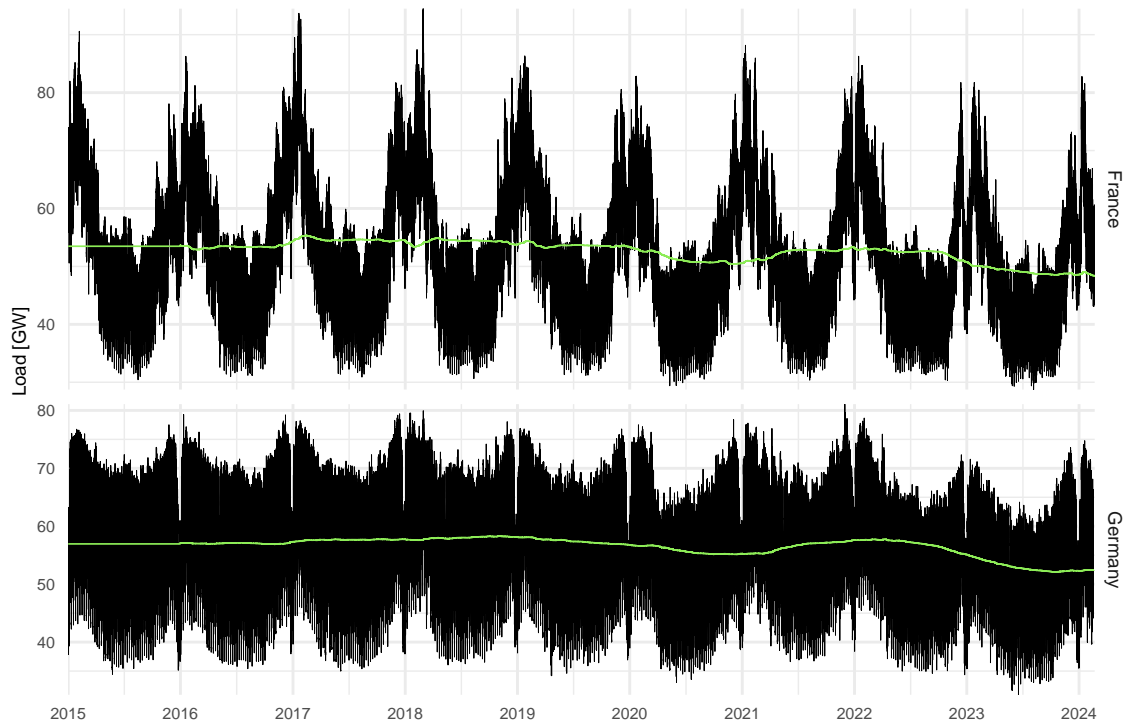


Figure 2: Hourly load (black) and yearly, i.e. 52 weeks, moving average load (green) from January 1st, 2015 to February 17th, 2024.

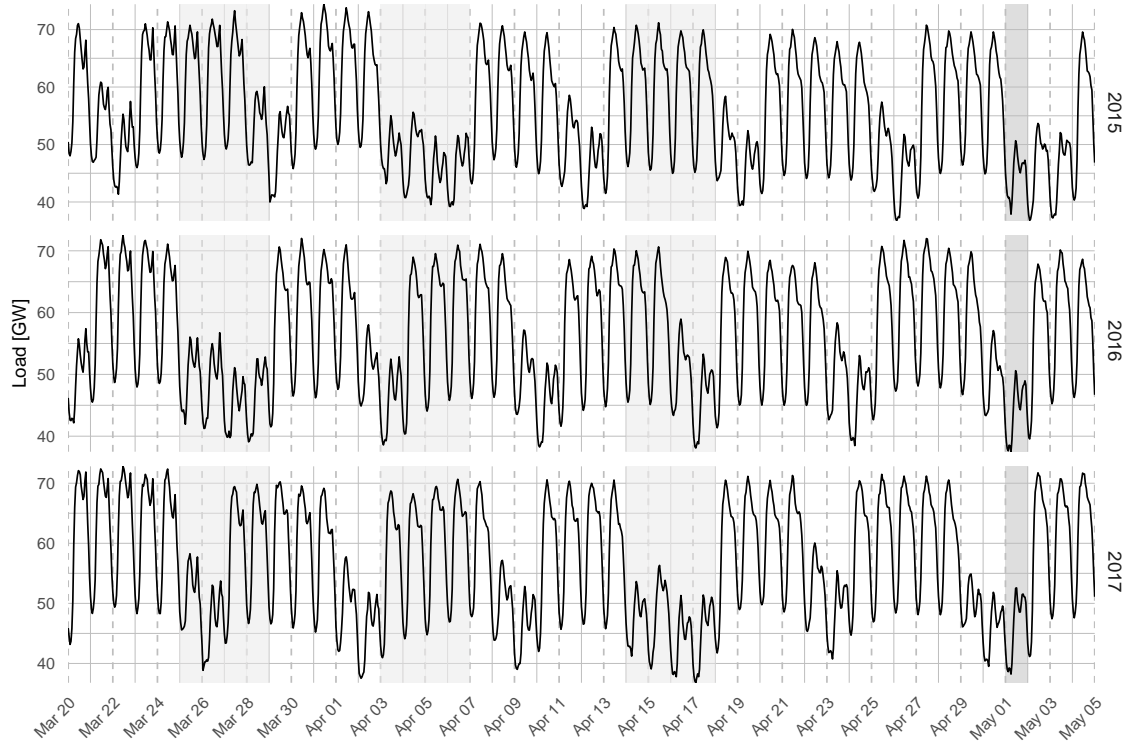


Figure 3: Hourly load in Germany in the Easter holiday time (March 1st to May 10th in 2016, 2017 and 2018) with holidays shaded in grey.

2.1. Calender Effects

The load profiles exhibit strong seasonal patterns across daily, weekly, and annual cycles, as shown by Figures 2 and 3. These patterns include lower load levels during summer compared to winter months, higher loads on weekdays compared to weekends, and lower loads at night compared to daytime. Additionally, on holidays load is reduced due to decreased work and industrial activity. This disruption to the typical weekly load pattern is evident in Figure 3, which shows the load time series for the Easter holiday time in Germany. Moreover, from Figure 2 we observe, that during the entire Christmas period load levels drop. Thus, besides single-day holidays, a winter holiday period encompassing December 18th to January 6th in every country is considered.

All calendar-based effects on load are known in advance, classifying them as deterministic. Their spatial level is national, as holidays are typically defined on the country level (see Tab. 1, l. 1).

2.2. Weather Effects

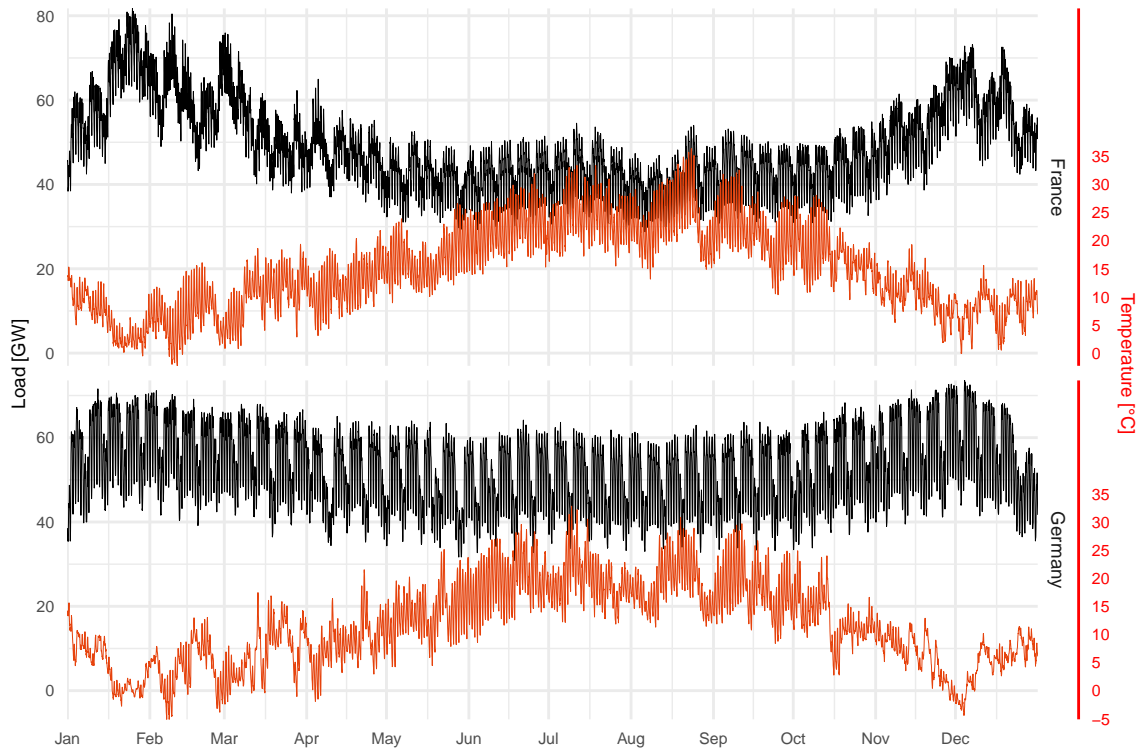


Figure 4: Hourly load (black) and temperature (red) in 2023.

Weather conditions, in particular, temperature significantly impact load due to its influence on electric heating and cooling. Typically, during summer, higher temperatures lead to increased load as cooling demands rise. Conversely, in winter, lower temperatures result in higher loads due to heating demands.

²While data from all European countries participating in ENTSOE was initially collected, some countries were ultimately excluded from the analysis due to data quality issues. This resulted in a final dataset encompassing data from 24 European countries: Austria, Belgium, Bulgaria, Czech Republic, Germany, Denmark, Estonia, Spain, Finland, France, Greece, Hungary, Italy, Lithuania, Latvia, Montenegro, Netherlands, Poland, Portugal, Romania, Serbia, Sweden, Slovenia, Slovakia.

This non-linear relationship between temperature and load has been confirmed through various studies, see e.g. the overview by [Verwiebe et al. \(2021\)](#); [Davis et al. \(2016\)](#) and the comprehensive European study by [Bessec & Fouquau \(2008\)](#) or [Bashiri Behmiri et al. \(2023\)](#); [Moral-Carcedo & Pérez-García \(2019\)](#); [Ziel \(2018\)](#); [Xie et al. \(2018\)](#) and is evident in Figures 4 for France. Notably, the sensitivity of load to temperature is low in Germany.

The uncertainty in weather time series is stochastic with pronounced seasonal patterns, including weekly and annual cycles. While temperatures are primarily determined by regional weather conditions, mid-term prevailing weather systems, such as high and low-pressure areas, can influence temperature across multiple countries in Europe. Consequently, weather effects on load are considered to have a national spatial level with transnational components (see Tab 1, l. 2).

In our probabilistic modeling approach, we capture this spatial property of weather effects by estimating point forecast models for temperatures at the country level but incorporating intra-country correlations for the probabilistic forecasts. By this, we account for the risk of Pan-European extreme weather scenarios on load. Examining how such extreme weather scenarios affect the temperature-sensitive load in France, in Section 6.3, will provide initial insights of their effect under similarly temperature-sensitive load across most European countries, e.g. due to the large-scale rollout of heat pumps.

2.3. Socio-Economic and Political Effects

Load is influenced by past observations in terms of its previous mid-term level. More precisely, random shocks on load, e.g. due to transnational factors like a financial crisis, carbon tax, decarbonization incentives, technological advancements, supply shortages, or large-scale migration caused by war, can cause permanent deviations from a predetermined equilibrium level, see [González Grandón et al. \(2024\)](#). Since the stochastic component in electricity demand is strongly tied to the economy, load inherits the prevalence of these shocks via transmission flows from key macroeconomic, socioeconomic and energy variables. Additionally, political legislation and incentives inducing prevailing structural changes influence equilibrium load levels either directly or through the beforementioned variables [Schneider & Strielkowski \(2023\)](#); [Narayan & Liu \(2015\)](#); [Hendry & Juselius \(2000\)](#); [Smyth \(2013\)](#).

Key macroeconomic drivers of electricity demand are, for instance, Gross Domestic Product, employment rate, Consumer Price Index and Industrial Production Index measuring economic well-being, purchasing power, and production output of manufacturing and utilities, see e.g. [González Grandón et al. \(2024\)](#). These macroeconomic variables, with GDP being a prime example, see [Kalhori et al. \(2022\)](#); [Harvey et al. \(2007\)](#), are generally recognized to exhibit persistent shifts in their level component. This has been, firstly, evidenced by the seminal work of [Nelson & Plosser \(1982\)](#) and mostly supported by revisiting studies, see e.g. [Gil-Alaña & Robinson \(1997\)](#); [Perron \(1997\)](#) among others. Socioeconomic and energy variables affecting load are, for instance, population size and fossil fuel prices or carbon taxes through industrial production, see e.g. [González Grandón et al. \(2024\)](#); [Moral-Carcedo & Pérez-García \(2019\)](#). Similar to macroeconomic variables, these factors are predominantly recognized to exhibit a permanent shift in levels.

Recent examples of political impacts on equilibrium load include load level increases driven by incen-

tives aimed at accelerating electrified heating and transportation to meet decarbonization goals, and load level decreases due to politically mandated COVID-19 lockdowns. Moreover, the political management of large-scale migration or exceptionally high industrial production in the armaments sector, caused by geopolitical conflicts, could result in mid-term changes in load levels.

For a literature overview on the unit root behavior in energy variables, we refer to [Smyth \(2013\)](#). For methodological approaches to measure the effect of economic and political shocks on energy variables, we refer to [Schneider & Strielkowski \(2023\)](#) and [Narayan & Liu \(2015\)](#).

Following the illustration of load levels in [Ziel \(2019\)](#), Figure 2 depicts hourly load beside the yearly moving average load in France and Germany. In both countries, the averaged load data exhibit gradual shifts in particular in the last four years.

Prevailing shifts in the level component of load make this process non-stationary. Recall that a non-stationary process exhibits fluctuations in its statistical properties (mean, variance, and autocorrelation) over time. By differencing the level time series, it can be stabilized. This form of non-stationarity is known as a unit root³.

Consequently, the underlying socio-economic and political state reflected in load time series follows a unit root stochastic process. Despite strong cross-border economic interdependence and a rise in pan-European legislation, national differences prevail. For instance, European countries handled the COVID-19 pandemic with varying approaches.

In our methodology, we account for this spatial property (see Table 1, l. 3) of the socio-economic and political effect on load by modeling it multivariate in all considered countries. Additionally, differently cross-country dependent models are considered for the underlying unit root of this effect. Besides a stationary model serving as a baseline for comparison, a cointegrated and individual unit root model are evaluated. Whereas the cointegrated model assumes only one underlying pan-European socio-economic and political unit root, the individual model assumes a specific unit root in the socio-economic and political state series of each country but with a Pan-European memory of past observations.

2.4. Autoregressive Effect

With weather and previous mid-term socio-economic and political effects on load explained, short to mid-term (hours to several weeks) autoregressive deviations persist in the calendar-based load pattern. Commonly, instantaneous external influences can impact load beyond their timeframe. For instance, even if weather conditions affecting heating or cooling subside, their impact on human behavior persists for several days, causing deviations in load patterns for the most recent lags, as well as lags of neighboring hours on the previous day and the previous week. Furthermore, major sporting events like the FIFA World Cup or the Olympics can cause short-term deviations in load patterns during match times and

³Our study compares unit root and non-unit root modeling of the socio-economic and political levels in load, deliberately bypassing formal unit root testing due to the ongoing research in this area, see e.g. [Schneider & Strielkowski \(2023\)](#), and the statistical complexities inherent in applying such tests to electricity time series. For a comprehensive assessment of unit root behavior in electricity time series, we recommend the literature reviews by [Schneider & Strielkowski \(2023\)](#); [Smyth \(2013\)](#).

the hours surrounding these events due to increased viewership and associated activities.

Autoregressive effects are stochastic and mostly national in their spatial level, thus point forecast autoregressive models are estimated at the country level. However, since the initiating causes of short-term external load effects can transcend national borders, inter-country correlations are considered for probabilistic forecasts.

2.5. The Confluence of Load Effects

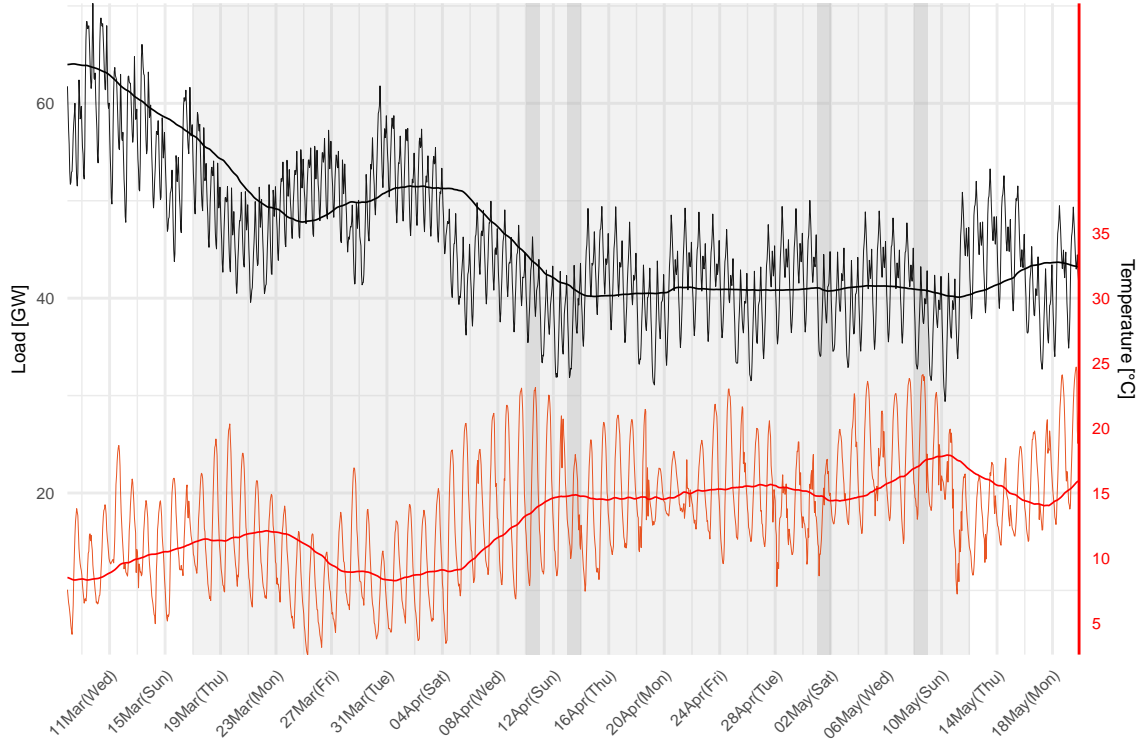


Figure 5: Hourly load (black) and temperature (red) and their weekly moving average in France from March 14th to May 19th, 2020 with the time of the first lockdown due to COVID-19 shaded in grey and holidays shaded in darkgrey.

Disentangling and interpreting the combined effect of the various factors impacting load presents a significant challenge in mid-term hourly load forecasting. Figure 5 provides an intuition of this complexity by illustrating hourly load and temperatures in France during the first COVID-19 lockdown. We observe a significant drop in load levels coinciding with a slight temperature increase in the days leading up to and at the beginning of the lockdown. During this time it is difficult to disentangle the load-reducing effect of rising temperatures from the socioeconomic lockdown effect, which likely caused the primary load reduction.

Further complicating the picture are several holidays within the lockdown period: Good Friday (April 10th), Easter Monday (April 13th), Labor Day (May 1st), and Victory in Europe Day (May 8th) (shaded in dark grey). These holidays presumably caused additional load reductions, making it even harder to isolate the individual effects. For example, on Easter Monday, the temperature decrease, which typically increases the load, might have been masked by the combined effects of reduced activity due to the holiday and the ongoing lockdown.

Imagine a future scenario where two risky drivers converge: a cold period in Europe, which might by then rely heavily on electric heating, experiencing a socioeconomic crisis. Such a situation could lead to a drastic deviation in load levels. Therefore, developing interpretable models is crucial to assess these risks in advance and ensure grid stability and energy security.

3. Primer On Statistical Models

3.1. Generalized Additive Models

Generalized Additive Models (GAM) are the main building blocks to combine the multifaceted stochastic and deterministic characteristics of load and form our forecasting model. Specifically, we choose GAMs that describe a response variable Y_t as an additive combination μ of smooth cubic B-splines $f_i : \mathbb{R}^m \rightarrow \mathbb{R}$ $f_i(\mathbf{X}) = \sum_{l=1}^{k_1} \dots \sum_{j=1}^{k_m} \beta_{i,...,j} b_l^1(x^1) \cdot \dots \cdot b_j^m(x^m)$ in the covariates $\mathbf{X}_t = (X_t^1, \dots, X_t^m) \in \mathbb{R}^m$, $t \in \{1, \dots, N\}$:

$$Y_t = o + \mu(\mathbf{X}_t) + \varepsilon_t, \quad \mu(\mathbf{X}_t) = f_1(\mathbf{X}_t) + f_2(\mathbf{X}_t) + \dots + f_M(\mathbf{X}_t) \quad (1)$$

where $o \in \mathbb{R}$, $\varepsilon_t \sim \mathcal{N}(0, \sigma_t)$.

For estimation⁴ a penalized least-squares objective with smoothing parameters $\lambda_i \in \mathbb{R}_{\geq 0}^m$ and a difference-based penalty on parameter deviation is applied:

$$\|\mathbf{Y} - \mathbb{X}\boldsymbol{\beta}\|^2 + \sum_{i=1}^M \lambda_i \mathcal{P}(f_i), \quad (2)$$

$$\mathcal{P}\left(\sum_{i=1}^k \beta_i b_i(x)\right) = \sum_{i=1}^{k-p} (\Delta^p \beta_i)^2 = \boldsymbol{\beta}^T S \boldsymbol{\beta}, \quad (3)$$

where $\mathbb{X}_t = (\mathbb{X}_{t,1}^1 \otimes \dots \otimes \mathbb{X}_{t,m}^1, \dots, \mathbb{X}_{t,1}^M \otimes \dots \otimes \mathbb{X}_{t,m}^M)$ for the tensor product \otimes on matrix space and $\mathbb{X}_{t,j}^l = (b_1^j(X_t^j), \dots, b_{k_j}^j(X_t^j))$ and Δ is the difference operator. The resulting smooth terms are named *P-splines*. For a so-called cyclic P-spline, terms are added to penalize deviation between the first and last coefficients, e.g. $(\beta_1 - 2\beta_n + \beta_{n-1})^2$ and $(\beta_2 - 2\beta_1 + \beta_n)^2$ for $p = 2$. The generalization of \mathcal{P} to multivariate splines penalizes parameter deviation individually for each marginal.

To select appropriate parameters β_i and smoothing parameters λ_i , minimization of criteria such as the generalized cross-validation (GCV) score or the unbiased estimator criterion (UBRE), REML or ML estimation, and variations thereof can be applied. For further insights on these criteria and methods of minimization, we refer to [Wood \(2006\)](#) or [Lepore et al. \(2022\)](#). GAM modeling and estimation methods are implemented in the R-package mgcv, see [Wood \(2006\)](#).

3.2. Probabilistic Vector Additive Autoregressive and State Models

To probabilistically forecast the stochastic drivers of load, three types of models are applied: Vector Autoregression (VAR), Vector Error Correction (VECM) and Vector Error-Trend-Seasonal (VETS) Models, whereby VAR and VETS models are applied in their univariate and multivariate form. In all three models, forecasts are generated by the dependence on past observations, specifically as weighted sums of autoregressive, differenced autoregressive and initial state components.

⁴Note that smooth functions f_1, \dots, f_M can only be identified and thus estimated in (1) up to a constant. Consequently, practical applications employ identifiability constraints, commonly $\mu(\mathbf{X}_t) = 0$ or $f_i(0) = 0$, see [Wood \(2006\)](#) for details.

VAR($\nu, \phi; p_{\max}$)	VECM($\nu, \Gamma, \Pi; r < n$)
$\mathbf{Y}_t = \nu + \sum_{k \in \mathcal{S}} \phi_k \mathbf{Y}_{t-k} + \epsilon_t$	$\Delta \mathbf{Y}_t = \nu + \Gamma \Delta \mathbf{Y}_{t-1} + \Pi \mathbf{Y}_{t-1} + \epsilon_t$
$\widehat{\mathbf{Y}}_{T+h T} = \nu + \sum_{k \in \mathcal{S}} \phi_k \widehat{\mathbf{Y}}_{T+h-k T} + \epsilon_{T+h}$ for $\epsilon_{T+h} \sim \mathcal{N}(0, \Sigma)$	$\widehat{\Delta \mathbf{Y}}_{T+h T} = \nu + \Gamma \widehat{\Delta \mathbf{Y}}_{T+h-1 T} + \Pi \widehat{\mathbf{Y}}_{T+h-1 T} + \epsilon_{T+h}$ for $\epsilon_{T+h} \sim \mathcal{N}(0, \Sigma)$
$\widehat{\mathbf{Y}}_{T+h-k T} = \mathbf{Y}_{T+h-k}$ for $h \leq k$	$\widehat{\Delta \mathbf{Y}}_{T+1 T} = \nu + \Gamma \Delta \mathbf{Y}_T + \Pi \mathbf{Y}_T$

Table 2: VAR model for a set of lags $\mathcal{S} \subset \{1, \dots, p_{\max}\}$. VECM for $\Pi = \alpha \beta^\top$ and $\beta^\top \mathbf{Y}_{t-1}$ a $r \times 1$ vector of stationary cointegrated relations.

For the multivariate autoregressive, thus VAR model (see Tab. 2, col. 1), maximum likelihood is applied for estimation and the set of lags is fixed to $\mathcal{S} = \{1, 2\}$. For the univariate autoregressive model (see Tab. 2, col. 1, for $\mathbf{Y}_t, \nu, \epsilon_t, \phi_t^\top \in \mathbb{R}^n, n = 1$) Post-Lasso OLS is applied, i.e. lags $p \in \mathcal{S} \subset \{1, \dots, p_{\max}\}$ are chosen by Lasso and OLS estimation is carried out for the resulting non-zero lags for bias reduction, see Lee et al. (2016).

For the VECM model (see Tab. 2, col. 2) maximum likelihood is applied for estimation. The reduced rank $r < n$ of the matrix Π captures the cointegrated unit root behavior of $\mathbf{Y}_t \in \mathbb{R}^n$. Cointegration vectors are represented by the columns of the matrix β . The remaining number of unit roots $n - r$ can be interpreted as joint underlying drivers of the non-stationary trend behaviors in \mathbf{Y}_t , see Jusélius (2009).

VETS(α)	VETS($\alpha, \gamma; m$)
$\mathbf{Y}_t = \mathbf{l}_{t-1} + \epsilon_t$	$\mathbf{Y}_t = \mathbf{l}_{t-1} + \mathbf{s}_{t-m} + \epsilon_t$
$\mathbf{l}_t = \mathbf{l}_{t-1} + \alpha \epsilon_t$	$\mathbf{l}_t = \mathbf{l}_{t-1} + \alpha \epsilon_t$
$\widehat{\mathbf{Y}}_{T+h t} = \mathbf{l}_T + \epsilon_{T+h}$ for $\epsilon_{T+h} \sim \mathcal{N}(0, \Sigma)$	$\mathbf{s}_t = \mathbf{s}_{t-m} + \gamma \epsilon_t$ $\widehat{\mathbf{Y}}_{T+h t} = \mathbf{l}_T + \mathbf{s}_{T+h-m} \lceil \frac{h}{m} \rceil + \epsilon_{T+h}$ for $\epsilon_{T+h} \sim \mathcal{N}(0, \Sigma)$

Table 3: Additive VETS models with level states $\mathbf{l}_t \in \mathbb{R}^n$, seasonal states $\mathbf{s}_t \in \mathbb{R}^n$, common smoothing parameters $\alpha, \gamma \in (0, 1)$ and periodicity m .

While for VAR models no assumption is imposed on the weights assigned to past observations, additive VETS models (see Tab. 3, col. 1-2), formulated by De Silva et al. (2010) and specified by Svetunkov et al. (2023), impose exponentially diminishing weights. This is obtained by applying exponential smoothing with respect to the additive decomposition of the univariate time series Y_t^1, \dots, Y_t^n into their states, i.e. level l_t^1, \dots, l_t^n and seasonal s_t^1, \dots, s_t^n component⁵. From the model formulation, it directly follows that each resulting univariate time series exhibits an individual non-stationary unit root behavior, i.e. by first-order and seasonal differencing a stationary white noise process remains. Thereby, the exponential decay of weights assigned to past observations is governed for all univariate time series by common smoothing parameters $\alpha, \gamma \in (0, 1)$. This can be interpreted as a common memory of deviations in equilibrium levels. For estimation, the implementation by Svetunkov et al. (2023) is applied and the trace of the covariance matrix of errors is minimized.

⁵In all VETS models considered in this work the trend component is assumed to be zero.

Probabilistic forecasts from the three models are obtained iteratively with sampled multivariate normal error terms $\epsilon_t \sim \mathcal{N}(0, \Sigma)$ with in-sample estimated covariance assuming zero mean

$$\hat{\Sigma} = \frac{1}{T-1} \sum_{i=1}^T \hat{\epsilon}_i \hat{\epsilon}_i^\top. \quad (4)$$

For the univariate VAR, the LASSO-based selection \mathcal{S} of relevant lags in $\{1, \dots, p_{\max}\}$ enables to implement each forecasting iteration with sparse matrix algebra, which greatly reduces calculation times.

4. Methodology

4.1. Modelling Concept

As detailed in Section 2.1, disentangling the combined influence of the various deterministic or stochastic and national or transnational load effects and obtaining interpretable models, in particular, in stochastic load effects, presents a significant challenge in mid-term hourly load forecasting. To address this challenge, we propose an interpretable model based on GAMs that integrates probabilistic VETS, VAR and VECM models to capture stochastic effects. The general process of the model is illustrated by the flowchart in Figure 8 and described in the subsequent. We will focus on the probabilistic components of the model in this section. A detailed explanation of the underlying point forecast model and parameter definitions can be found in our previous work, see [Zimmermann & Ziel \(2024\)](#).

Variable	Processed Information	Available Timeframe
$\mathbf{X}_t^{\text{Cal-based}}$	hourly calender-based information, time of the day, week, year, interactions, holidays and holiday period	$t = 1, \dots, T + H$
$\mathbf{X}_t^{\text{Temp}}$	hourly average temperatures in most populated cities	$t = 1, \dots, T$
$\mathbf{X}_t^{\text{Season}}$	hourly time of the day, time of the year and interaction	$t = 1, \dots, T + H$

Table 4: Input variables $\mathbf{X}_t^m \in \mathbb{R}^n$ of the proposed probabilistic load forecasting model.

Let $\mathbf{Y}_t \in \mathbb{R}^n$ and $\mathbf{X}_t^{\text{Temp}} \in \mathbb{R}^n$ (see Tab 4, l. 2) be the observed load and temperature in n considered countries at time $t = 1, \dots, T$, respectively. Additionally, we have access to deterministic calender-based information about seasonalities and holidays $\mathbf{X}_t^{\text{Cal-based}} \in \mathbb{R}^n$ (see Tab 4, l. 1) for the extended horizon $t = 1, \dots, T + H$. It is the objective to probabilistically forecast load over a mid-term prediction horizon H of several weeks to one year by the modeling equations (5)-(7) for countries $i = 1, \dots, n$:

$$Y_t^i = o + \underbrace{\mu^{i, \text{Cal-based}}(X_t^{i, \text{Cal-based}})}_{\text{smooth terms in deterministic calendar effects}} + \underbrace{\mu^{i, \text{Temp}}(X_t^{i, \text{Temp}})}_{\text{smooth terms in stochastic weather effects (i)}} \quad (5)$$

$$+ \underbrace{\mu^{i, \text{SocEconPol-State}}(X_t^{i, \text{SocEconPol-State}})}_{\text{smooth terms in stochastic socio-economic and political effects (ii)}} \quad (6)$$

$$+ \underbrace{\mathcal{E}_t^i}_{\text{stochastic autoregressive effects (iii)}} \quad (7)$$

The variable representing socio-economic and political states, $\mathbf{X}_t^{\text{SocEconPol-State}} \in \mathbb{R}^n$, is obtained in step (ii) of the model and is therefore not available as initial information.

(i) Probabilistic temperature forecast: Since accurate weather and satellite imagery-based temperature forecasts are not feasible for mid-term horizons, we rely on deterministic seasonalities and stochastic autoregressive components as inputs for probabilistic temperature modeling (see Figure 8 on the left-hand-side). Temperatures $\mathbf{X}_t^{\text{Temp}}$ are first, smoothed by VETS models with fixed smoothing parameters. By this, fluctuations explained by short-term weather conditions are removed. To account for the primarily national spatial level of weather (see Tab. 1, l. 2), smoothed temperatures $\widetilde{\mathbf{X}}_t^{\text{Temp}}$ are then modeled by country-specific GAMs in the deterministic seasonalities, i.e. the time of the day and the time of the year. To capture the stochastic autoregressive effect in temperatures, we employ univariate VAR models on the residuals of each country-specific two-step GAM. Cross-country correlations of the residuals from the resulting nationally modeled temperatures are high, in particular, for neighboring countries (see Fig. 6), implying an underlying pan-European weather system affecting the temperatures in multiple countries. To account for this second spatial property of weather (see Tab. 1, l. 2), nationally modeled temperatures are probabilistically forecasted incorporating an estimated intra-country residual covariance. Probabilistic multivariate forecasts of $\widetilde{\mathbf{X}}_t^{\text{Temp}}$ for the mid-term horizon $t = T + 1, \dots, T + H$ result by summing the autoregressive probabilistic forecasts and the two-step GAM point forecasts.



Figure 6: The in-sample correlation matrix $\widehat{\text{Corr}}(\epsilon_t^{\text{Temp}})$ for t , from February 6th, 2019 to February 1st, 2023 and smoothing parameter $\alpha = 1/24$.

(ii) Probabilistic socio-economic and political state forecast: To probabilistically forecast the socio-economic and political state (see Figure 8 middle part), firstly, load is modeled country-specific by GAMs from the smoothed temperatures obtained in (i) and deterministic seasonal and holiday information. Since these GAMs do not capture the unit root socio-economic and political state

effects, they remain in their residuals. Thus, secondly, to account for the spatial and uncertainty properties of these effects (see Tab. 1, l. 3), three types of models with differing assumptions on an underlying unit root and cross-country dependencies are applied to the GAMs residuals. As a base case for comparison, the VAR model (see Tab 2, col. 2) that assumes no unit root in the data is applied. In the VAR model cross-country effects are incorporated by multivariate modeling (i.e. the state of one country is affected by the states of all other countries). As the second model, the VECM (see Tab 2, col. 2) is applied. In our application of the model, we assume⁶ that there is one joint underlying unit root for the n country-specific states time series, i.e. that there is one pan-European socio-economic and political non-stationary trend fully explaining the non-stationarity of all country-specific state series. As the VAR model, the VECM incorporates cross-country effects by multivariate modeling. As third model, we use a VETS approach (see Table 3, col. 2) to model the socio-economic and political states. This model assumes a unit root in the state series of each country with a common smoothing parameter α , i.e. a common memory of past observations. While the model is estimated jointly, it assumes no direct influence of socio-economic and political states between countries. Since for all three models, cross-country correlations of the residuals are high (see Fig. 7 for VECM and 23, 24 for VAR, VETS in Appendix A) they are incorporated for probabilistic forecasting of all three models.

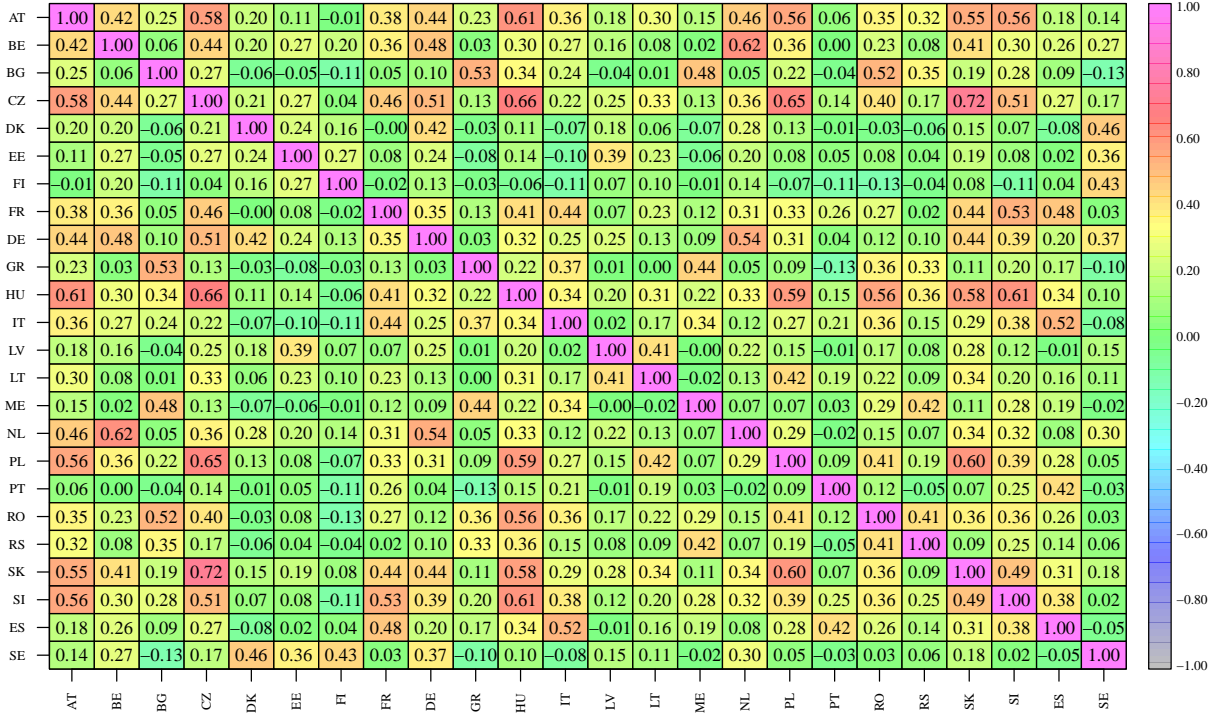


Figure 7: The in-sample correlation matrix $\widehat{\text{Corr}}(\epsilon_{\tau=1,\dots,T/(7 \times 24)}^{\text{VECM}})$ for τ from February 6th, 2019 to February 1st, 2023.

(iii) Probabilistic load forecast:

⁶Different numbers of cointegration vectors have been tested in an in-sample hyperparameter study, with decreasing error measures for an increasing number of cointegration vectors. The lowest errors were observed with $n - 1$ cointegration vectors, indicating the presence of one underlying unit root.

Lastly, the stochastic autoregressive effect of load is captured (see Figure 8 right-hand-side). For this, load is modeled again by country-specific GAMs with deterministic seasonal and holiday information, smoothed temperature, and, additionally, with the fitted socio-economic and political state from step (ii) as inputs. By using country-specific GAMs, we regard the impact of these inputs on load as national. This approach is reasonable for calendar-based and temperature effects. For example, different nationalities have specific calendar-based behaviors, such as common siesta times, peak working hours, and holidays, which do not affect the load in other countries. Moreover, countries vary in their use of electric heating or cooling and thus temperature sensitivity in load, as shown in Figure 4 comparing Germany and France. For the socio-economic and political states, cross-country influences on load are plausible due to the increasing interconnection of European power grids. However, this is accounted for even with country-specific GAMs, since the state variables are modeled multivariately, as explained in (ii).

In these GAMs residuals, the short to mid-term stochastic autoregressive effects remain. Thus, as for temperature modelling, we employ univariate VAR models on the residuals of each country-specific GAM and capture the transnational spatial property of the autoregressive component (see Tab. 1, l. 4) by forecasting it probabilistically with an estimated intra-country residual covariance⁷. Finally, forecasted load distributions are obtained as the sum of the GAM point and VAR probabilistic forecasts for each country with the temperature and state forecasts from (i) and (ii).

Note that a joint distribution of residuals from the three models (i) - (iii), i.e. a dependence between temperature, socio-economic and political and autoregressive scenarios, was not considered reasonable, as confirmed by estimated in-sample correlations (see Fig. 28 - 30 in Appendix A).

4.2. Modeling, Estimation and Forecasting Specifications

In the subsequent, the specific modeling equations, parameter choices along the estimation and forecasting methods applied to obtain the probabilistic temperature, socio-economic and political states and load forecasts, described in (i), (ii) and (iii), respectively, are defined. An overview of input variables is given in Tabel 4. For a precise definition of all variables, we refer to the detailed explanation of the corresponding point forecasting model in our previous work, see [Zimmermann & Ziel \(2024\)](#).

4.2.1. Probabilistic Temperature Model:

To probabilistically forecast smoothed temperatures, the following modeling equation is applied for countries $i = 1, \dots, n$:

$$\tilde{X}_t^{i,\text{Temp}} = o^{\text{Temp}} + \mu^{i,\text{Season}}(X_t^{i,\text{Season}}) + \varepsilon_t^{i,\text{Temp}}, \quad (8)$$

$$\varepsilon_t^{i,\text{Temp}} \sim \text{VAR}_{\text{Lasso}}(\nu, \phi^i; p_{\max}) \quad (9)$$

for $\mu^{i,\text{Season}}(X_t^{i,\text{Season}})$ smooth terms in daily and yearly seasonal information (see Tab. 4, l. 3).

⁷Corresponding correlation matrices can be found in Figures 25, 26, 27 in Appendix A

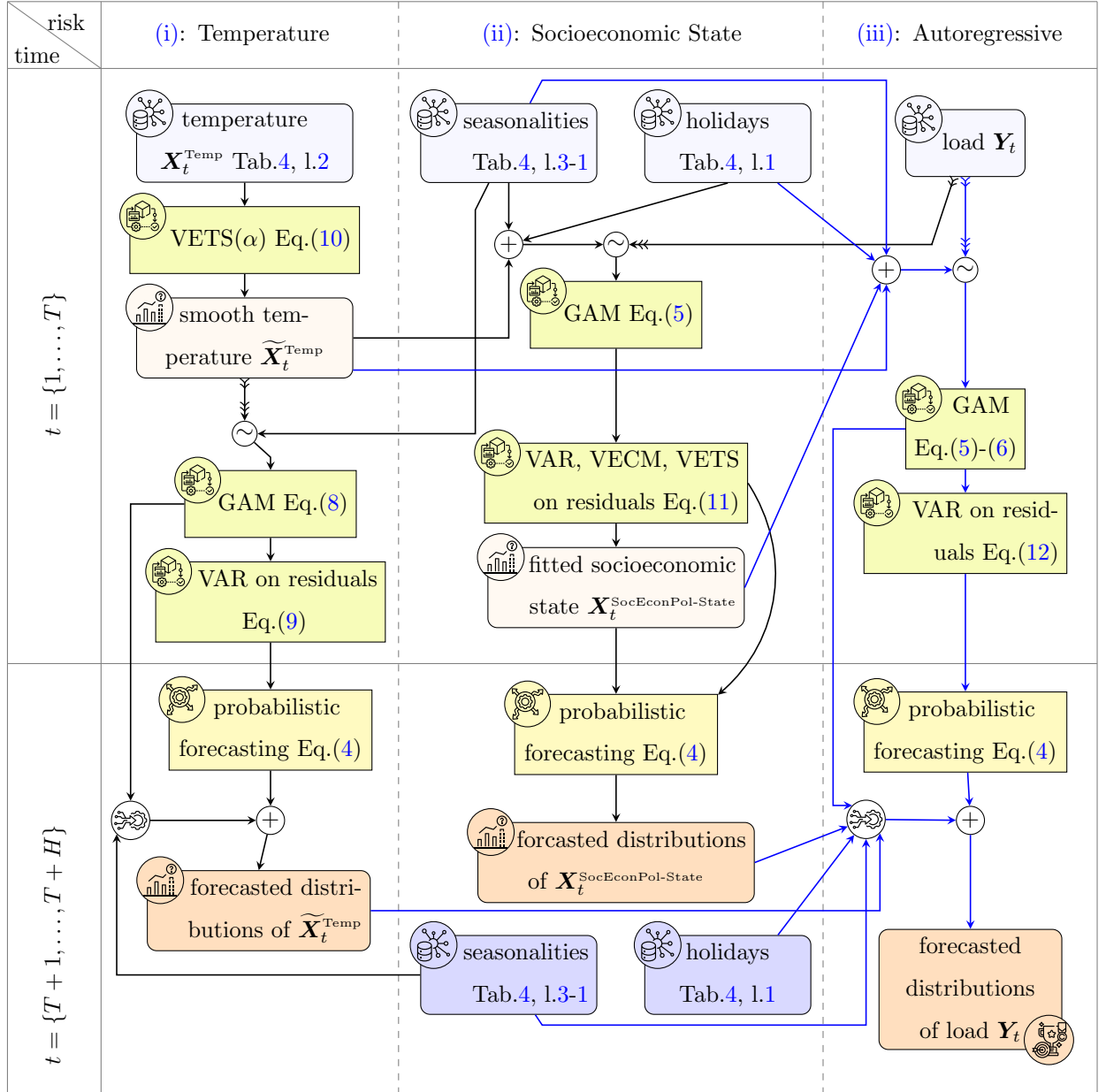


Figure 8: Flowchart representing the general process of the probabilistic load forecasting model with temperature, socio-economic and political state and autoregressive sources of risk resulting in multivariate distributions $\widehat{F}_{T+1}(\mathbf{Y}_{T+1}), \dots, \widehat{F}_{T+H}(\mathbf{Y}_{T+H})$. The external input information is framed by blue boxes and the output of models by orange boxes. Thereby, lighter shades are used for in-sample times and darker shades for out-of-sample times. Models are framed by yellow boxes. By blue lines, the inputs and models leading to the final load forecasts are marked.

Smooth terms in $\mu^{i,\text{Season}}$ are estimated as penalized cyclic cubic B-spline according to (2) with details specified in [Zimmermann & Ziel \(2024\)](#). Parameter estimation and probabilistic forecasting of (9) is carried out as specified in as specified in Tab. 2, col. 1 and (4) by Post-Lasso with $\nu = 0$ and $p_{\max} = 4 \times 24 \times 7$.

For each country, the above-described modeling procedure is applied to two smoothed temperature time series $\tilde{\mathbf{X}}_t^{i,\text{Temp}_1,2}$:

$$\tilde{\mathbf{X}}_t^{\text{Temp}_1,2} \sim \text{VETS}(\alpha_{1,2}) \quad (10)$$

for $\alpha_1 = 1/24$ and $\alpha_2 = 1/(14 \times 24)$ and VETS according to Tab. 3, col. 1. By this, a temperature time series with more variation⁸ and a shorter dependence on past temperatures ($\alpha_1 = 1/24$) and a smoother temperature time series with a longer dependence on past temperatures is considered ($\alpha_2 = 1/(14 \times 24)$).

4.2.2. Probabilistic Socio-Economic and Political State Model:

Three models, the VAR, VECM and VETS are applied and compared to probabilistically forecast the socio-economic and political state:

$$\mathbf{r}_\tau \sim \{\text{VAR}(\boldsymbol{\nu}, \boldsymbol{\phi}; \mathcal{S}), \text{VECM}(\boldsymbol{\nu}, \boldsymbol{\Gamma}, \boldsymbol{\Pi}; r < n), \text{VETS}(\alpha, \gamma; m)\} \quad (11)$$

for the temporal aggregation $\mathbf{r}_\tau = 1/|C| \sum_{c \in C} \boldsymbol{\varepsilon}_{7S(\tau-1)+c}$ of residuals $\boldsymbol{\varepsilon}_t$ of GAMs in (5). By this aggregation, residuals for hours from 8:00 to 19:00 for each working day of the week⁹, i.e. $C = \bigcup_{n=0}^4 \{8, \dots, 19\} + nS$, are averaged and the frequency of $\boldsymbol{\varepsilon}_t$ is reduced to a weekly interval.

For estimation and probabilistic forecasting of \mathbf{r}_τ methods, as specified in Section 3.2 with $\boldsymbol{\nu} = 0, \mathcal{S} = \{1, 2\}, r = n - 1$, an annual seasonality $m = 52$ and constant covariance matrix estimated according to (4) are applied. The temporal aggregation renders computation times in estimation and forecasting feasible. The information loss from this aggregation is mitigated by a specific setup of the smooth terms $\mu^{i,\text{SocEconPol-State}}$ in (6), as explained in [Zimmermann & Ziel \(2024\)](#).

For VAR and VECM, the socio-economic and political state $\mathbf{X}_t^{\text{SocEconPol-State}}$ is retrieved as linear interpolation from \mathbf{r}_τ with extended boundaries, i.e. $\mathbf{X}_t^{\text{SocEconPol-State}} = \mathbf{r}_{\tau_1}$ and $\mathbf{X}_t^{\text{SocEconPol-State}} = \mathbf{r}_{\tau_T}$ for $t < \min(C)$ and $t > \max(C) + (7 \times 24)\tau_T$, respectively. For the VETS model the fit and forecast of the level component \mathbf{l}_τ such that $\mathbf{r}_\tau \sim \text{VETS}(\alpha, \gamma; m)$ are retrieved and linearly interpolated with extended boundaries to obtain $\mathbf{X}_t^{\text{SocEconPol-State}}$.

4.2.3. Probabilistic Load Model:

Finally, load is forecasted probabilistically by the modeling equations (5)-(7), where in (7) the remaining uncertainty, i.e. the stochastic autoregressive effect, is incorporated by:

$$\boldsymbol{\varepsilon}_t^{i,\text{AR}} \sim \text{VARLasso}(\nu, \boldsymbol{\phi}^i, p_{\max}) \quad (12)$$

⁸Figure 6 only depicts residual correlations for $\alpha_1 = 1/24$, since the effect of temperature on load is mostly explained by smoothed temperatures $\tilde{\mathbf{X}}_t^{\text{Temp}}$ in this α . A similar Figure can be found for the smoothing parameter $\alpha_2 = 1/(14 \times 24)$ in Appendix A (see Fig. 22).

⁹This choice aligns with the peak load definition commonly used in European electricity markets for trading electricity futures.

Estimation and forecasting is carried out as specified in Tab. 2, col. 1 with Post-Lasso, $\nu = 0$, $p_{\max} = 8 \times 24 \times 7$ and covariance estimated according to (4).

5. Forecasting Study and Evaluation Design

To evaluate the proposed probabilistic load forecasting model we conducted a rolling window forecasting study comparing all three model options for the socio-economic and political state (**VAR**, **VECM**, **VETS**). For the study, more than 8 years of load data, from January 2015 to February 2024 were used. In-sample data in each forecasting experiment comprised 4 years of data, thus $4 \times 365 \times 24$ observations.

The forecasting horizon is chosen as 52 weeks, i.e. $H = 168 \times 52$. Due to the high overlap of hourly forecasts for a horizon of 52 weeks, the forecasting experiments of a study are highly correlated. Consequently, with each forecasting experiment the window of in-sample observations is rolled forward by one month, with forecasts always starting at 9 a.m. on the first day of each month. This results in, $N = 50$ experiments. In each experiment, 200 simulations are carried out for probabilistic forecasting.

As data preprocessing, single outliers in the load data are adjusted by a lasso-based estimate for observation dummies in a linear regression of load against its running median.

We assess forecasting accuracy using two common proper scoring rules for probabilistic forecasts: the pinball loss and the Continuous Ranked Probability Score (CRPS), see [Koenker & Bassett \(1978\)](#); [Gneiting & Raftery \(2007\)](#). These metrics are frequently employed in the field, as demonstrated by GEFCCOM [Hong et al. \(2016\)](#). Additionally, we evaluate model calibration through coverage plots. To evaluate and interpret weather, socio-economic and political and autoregressive risk, plots depicting the effect of extreme scenarios in each effect on load are analyzed. In addition, quantile fan plots and trajectory plots for forecasted load are discussed.

6. Results and Interpretation

6.1. Accuracy and Calibration

Evaluating calibration accuracy in terms of the averaged CRPS (see Tab. 10), we observe that in most countries the **VAR** has the lowest CRPS, followed narrowly by **VECM**, whereby the difference of CRPS remains low between all three models. Similarly, the difference in the pinball loss is low between all three considered models in France and Germany, see Figure 9. Thus, without significance testing on the difference of both metrics, no conclusions on the best-performing model can be drawn.

In France and Germany, the **VAR** and **VETS** models, respectively, have the lowest CRPS. Consequently, the following coverage plots for France and Germany in Figures 11-14 focus on these models.

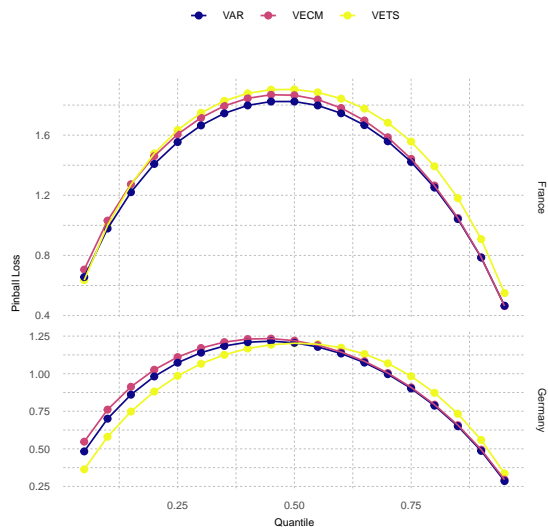


Figure 9: Pinball loss averaged over the forecasting horizon $1, \dots, H$ and experiments $1, \dots, N$.

	VAR	VECM	VETS
Austria	0.246	0.256	0.257
Belgium	0.343	0.338	0.332
Bulgaria	0.202	0.202	0.223
Czech Rep.	0.234	0.240	0.248
Denmark	0.163	0.161	0.163
Estonia	0.039	0.039	0.043
Finland	0.394	0.394	0.406
France	2.664	2.733	2.824
Germany	1.764	1.811	1.743
Greece	0.329	0.328	0.351
Hungary	0.194	0.195	0.197
Italy	1.416	1.416	1.732
Latvia	0.029	0.029	0.030
Lithuania	0.053	0.053	0.060
Montenegro	0.030	0.030	0.029
Netherlands	0.745	0.745	0.671
Poland	0.542	0.542	0.573
Portugal	0.197	0.197	0.220
Romania	0.266	0.266	0.264
Serbia	0.238	0.238	0.248
Slovakia	0.131	0.131	0.136
Slovenia	0.076	0.076	0.088
Spain	1.092	1.092	1.131
Sweden	0.670	0.670	0.692
Sum	12.057	12.183	12.663

Figure 10: Forecasting accuracy in terms of CRPS averaged over the forecasting horizon $1, \dots, H$ and experiments $1, \dots, N$ in GW for 24 European countries. The color scheme transitioning from red to yellow and green indicates models ranging from low to high accuracy. The best model for each country is marked by bold writing.

Comparing VETS and VAR in Figures 11-12 on the coverage averaged for each hour of the day, we observe that the former, is better calibrated, with only little deviations from the bisector lines for the morning to early afternoon hours and moderate deviations for the night hours. In contrast, VAR underestimates for all hours of the day, in particular, for quantiles $q \leq 75\%$. A similar result can be found for VECM in Appendix B (see Fig. 31).

Examining Figures 13-14 on the coverage averaged for the first and last two weeks of the one-year ahead forecasting horizon, we observe, as expected for iterative probabilistic forecasting, that calibration is better at the beginning of the horizon, with a tendency to underestimate towards the end. For the VAR a larger discrepancy in calibration accuracy between the beginning and end of the horizon is observed. Similar results are observed for the VECM model in Appendix B (see Fig. 32).

Comparing coverage plots in Figures 11-14 to CRPS values in Table 10 for the French data, we note that calibration of VETS is better, while CRPS of VAR is lower. This suggests, that if VETS over or underestimates, the deviation to the actual value averaged over the entire horizon is high. This can be attributed to the following: For the VETS model, a constant state forecast is incorporated into the GAM models (see Eq. (6)). If this state forecast over or underestimates, deviations will accumulate with each forecasting step throughout the horizon. In contrast, the state forecast of the VAR model, which assumes no unit root, converges to zero throughout the horizon.

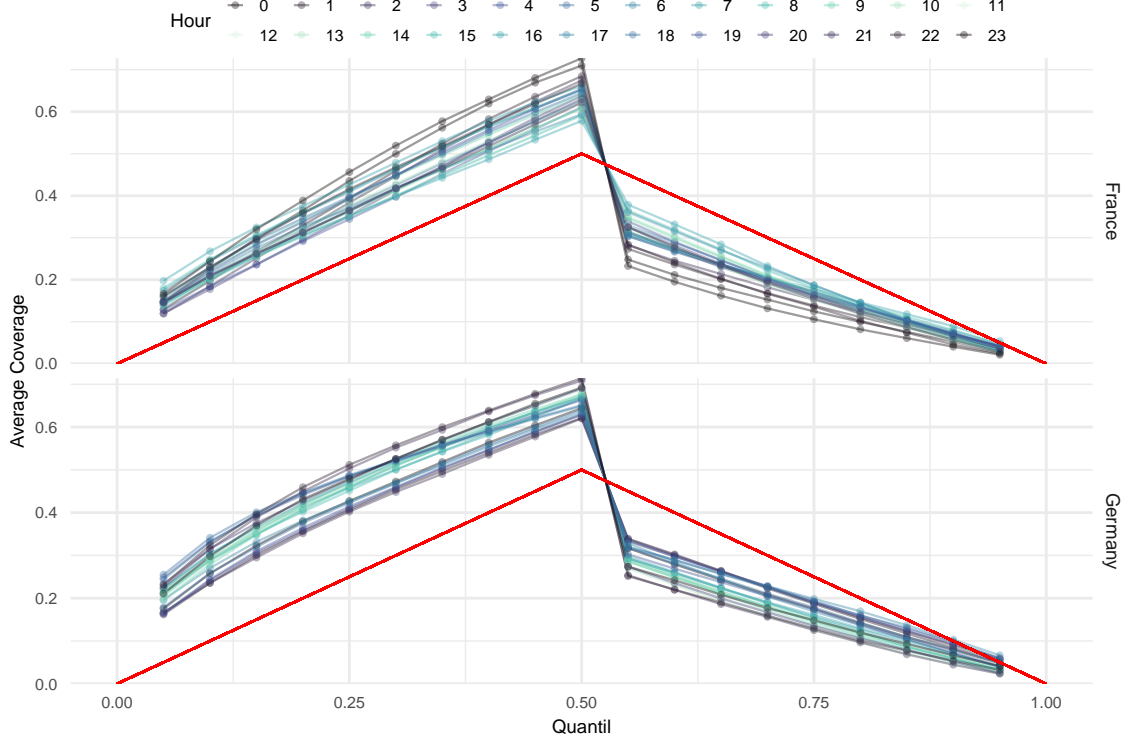


Figure 11: The frequency of underestimations ($q \leq 0.5$) and overestimation ($q > 0.5$) for quantiles $q = 5\%, \dots, 95\%$ of **VAR** in $N = 50$ forecasting experiments averaged for each hour of the day for France and Germany.

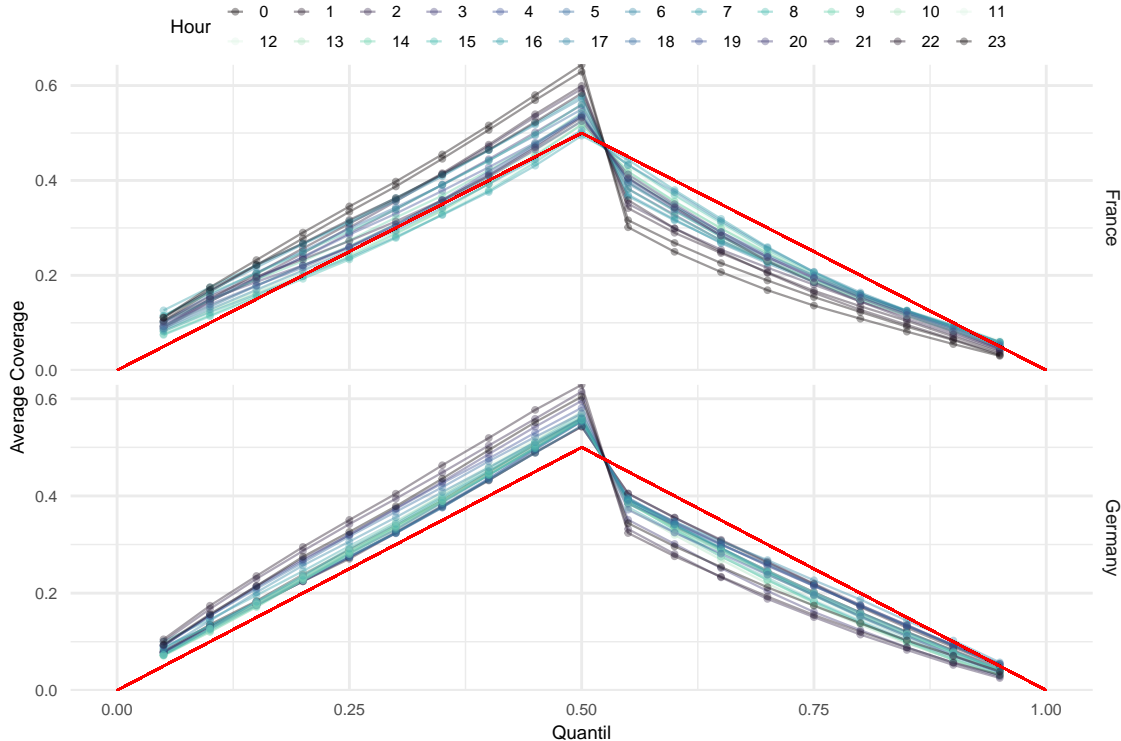


Figure 12: The frequency of underestimations ($q \leq 0.5$) and overestimation ($q > 0.5$) for quantiles $q = 5\%, \dots, 95\%$ of **VETS** in $N = 50$ forecasting experiments averaged for each hour of the day for France and Germany.

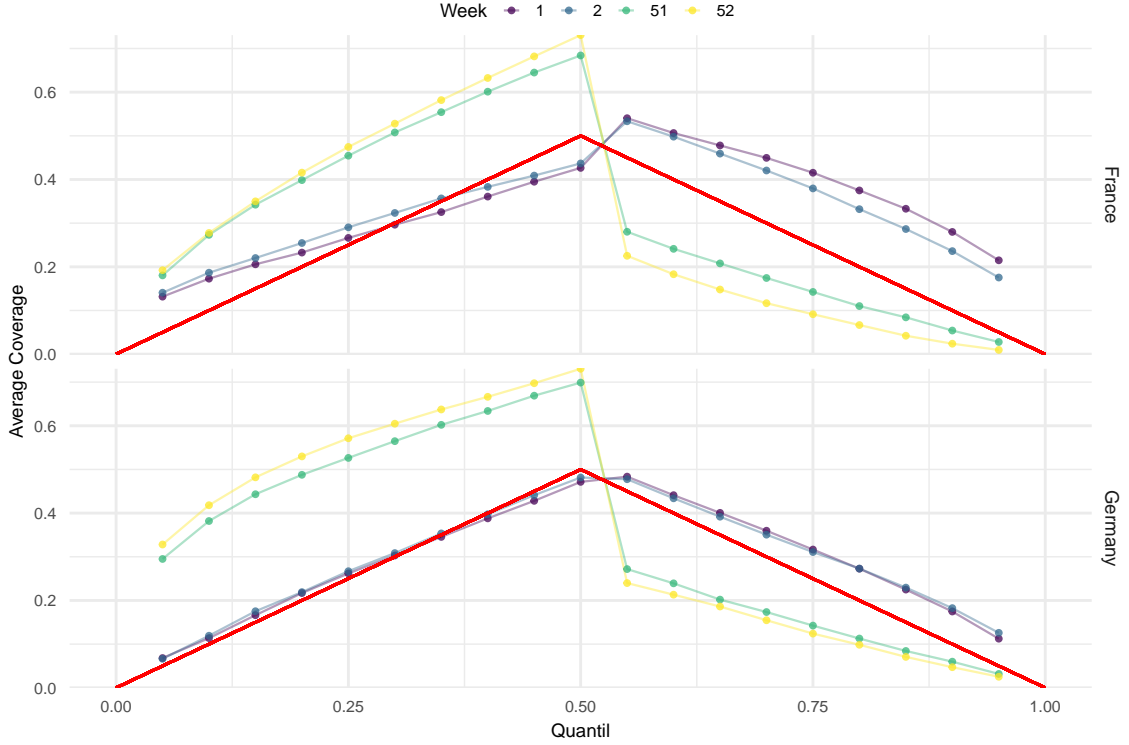


Figure 13: The frequency of underestimations ($q \leq 0.5$) and overestimation ($q > 0.5$) for quantiles $q = 5\%, \dots, 95\%$ of **VAR** in $N = 50$ forecasting experiments averaged for the first and last two weeks in the forecasting horizon for France and Germany.

6.2. Trajectory and Quantile Plots

Considering the calibration results for France and Germany (see Section 6.1) and the interest in the unit root effect of the mid-term socio-economic and political state, i.e. a persistent continuation of state levels in the prediction horizon, for risk assessment, the figures in this and the subsequent section will focus on the **VETS** model. Similar figures for the **VAR** model, which show only slightly different results, are available in Appendix B (see Fig. 33 - 39). In all figures, the forecasting experiment for $N = 50$ with in-sample data from February 6th, 2019 to February 1st, 2023 and the one-year ahead forecasting until January 31st, 2024 is depicted.

Figures 15 - 16 illustrate the ability of our model to capture transnational dependencies. These figures display three randomly sampled load forecast trajectories in France and Germany in the first two weeks and the last two weeks of the one-year horizon. Especially, from Figure 16 the alignment of higher and lower load levels in one country with similar trends in the other country is evident. Notably, the variation between trajectories increases towards the end of the horizon as expected for our iterative forecasting approach.

Figures 17 - 18 show the corresponding forecast quantiles. Consistent with the trajectory plots, we observe an increase in variation, particularly for France, towards the end of the forecasting horizon. The range between the 5th and 95th percentile for France expands to approximately 35 GW, compared to 25 GW for Germany. This suggests that load in France is more susceptible to stochastic effects. A likely explanation for this is a higher sensitivity to temperature fluctuations in France.

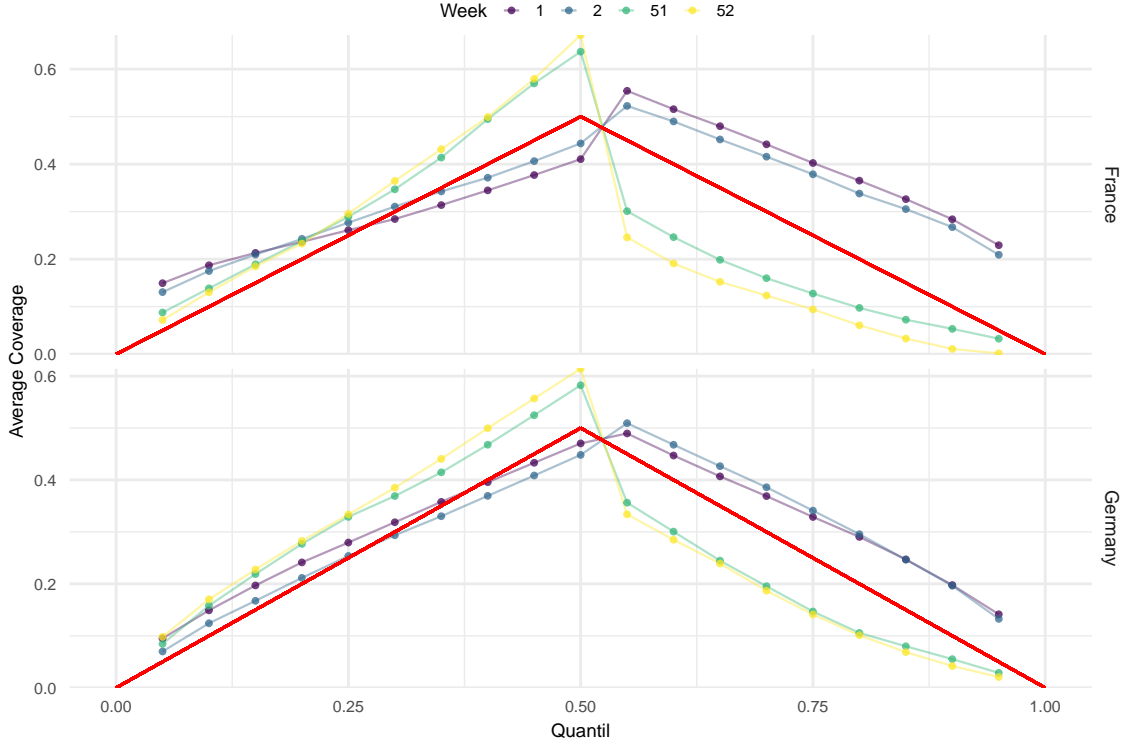


Figure 14: The frequency of underestimations ($q \leq 0.5$) and overestimation ($q > 0.5$) for quantiles $q = 5\%, \dots, 95\%$ of VETS in $N = 50$ forecasting experiments averaged for the first and last two weeks in the forecasting horizon for France and Germany.

An underestimation of all quantiles of the actual load in France during the week of February 7th to February 13th (see Fig. 17) could be attributed to two factors. Firstly, the forecasting period began with temperatures that were relatively moderate for winter in France but then fell to negative values, reaching a yearly low for 2023 around this week (see Fig. 4). This drop in temperatures could not be captured by quantiles of a week of iterative probabilistic forecasting with error sampling. Additionally, the GAM model in equations (5) - (6) might underestimate temperature effects by incorporating them into the deterministic yearly seasonal component, i.e. by assigning them to the variation in load between winter and summer.

6.3. Risk Scenario Analysis and Interpretation

A key strength of our load forecasting model lies in its interpretability. By this, we can identify the transmission of the multifaceted factors influencing load. Specifically, our model allows us to deconstruct the combined effect of various load drivers, taking their uncertainty and spatial dependencies into account.

To analyze the combined effect of extreme risk scenarios on load, we determined minimal and maximal trajectories for the stochastic temperature, socio-economic and political state and autoregressive components in our forecasting model. For this, we selected the trajectory that produced the largest underestimation and overestimation of the 5th and 95th percentile of their probabilistic forecasts, respectively, when summed across all time steps in the year-ahead horizon. Figure 19 depicts the corresponding temperature and socio-economic and political state trajectories, along with a medium trajectory, calcu-

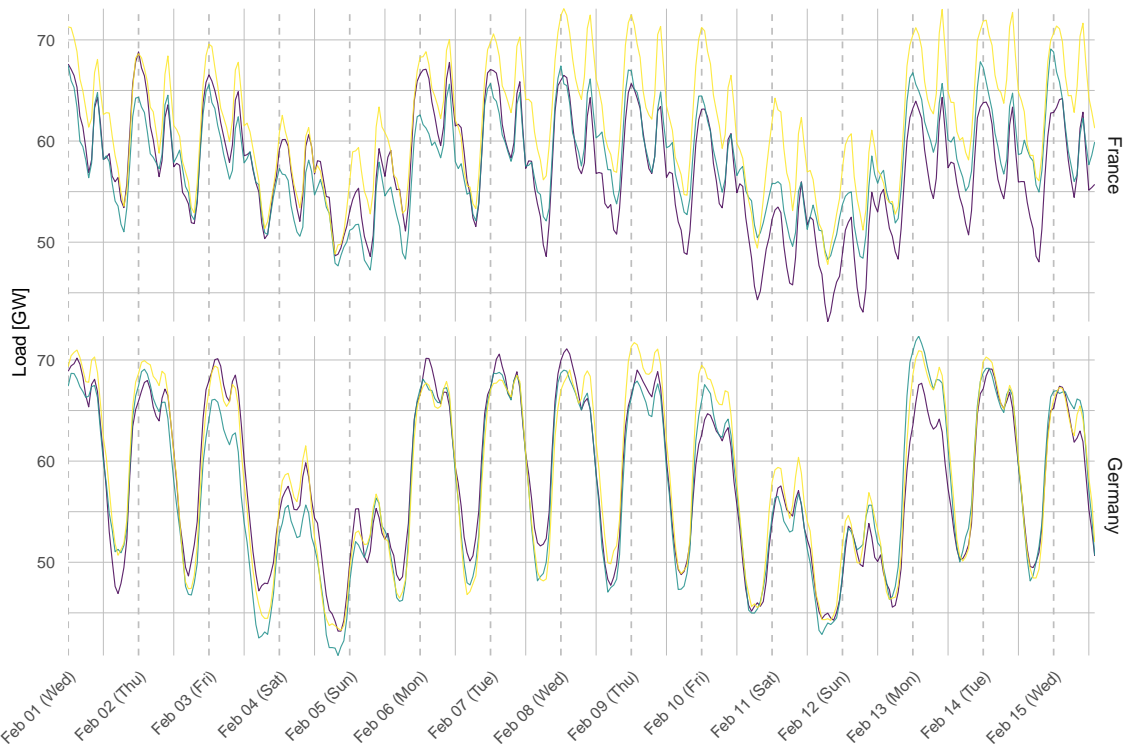


Figure 15: Three sampled load trajectories for the **VETS** model (forecasting experiment $N = 50$) in France and Germany forecasting the first two weeks of the one-year forecasting horizon (February 1st, 2023 to February 15th, 2023).

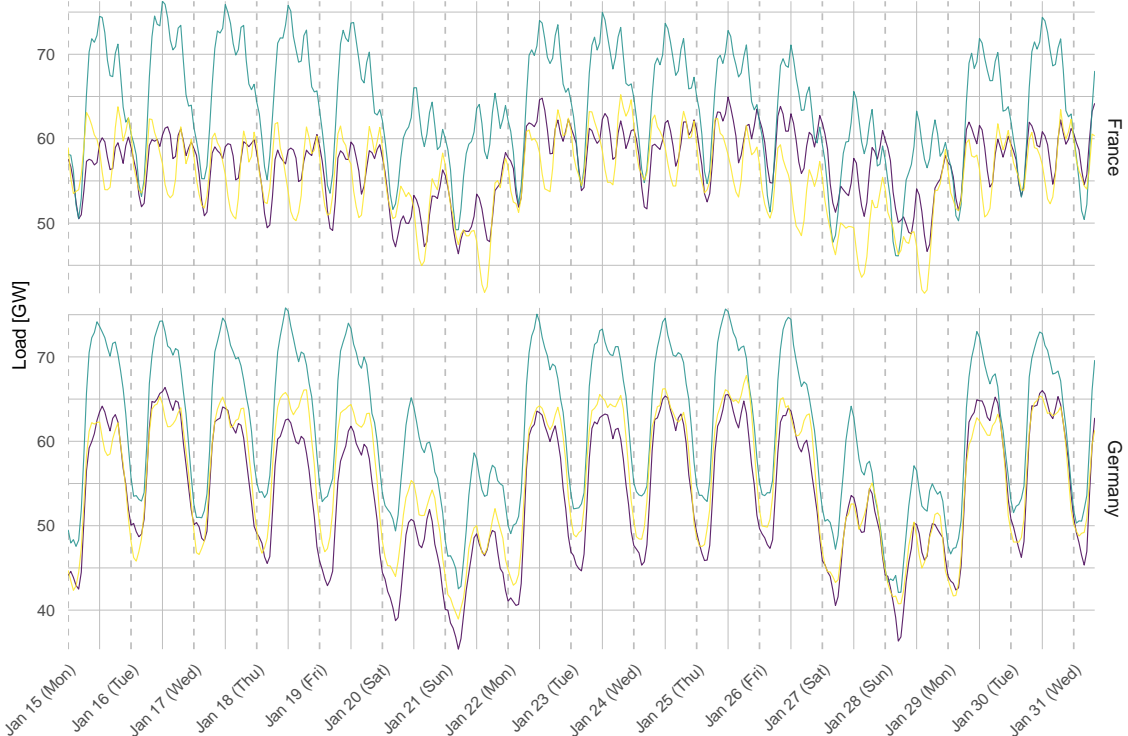


Figure 16: Three sampled load trajectories from the **VETS** model (forecasting experiment $N = 50$) in France and Germany forecasting the last two weeks of the one-year forecasting horizon (January 15th, 2024 to January 31st, 2024).

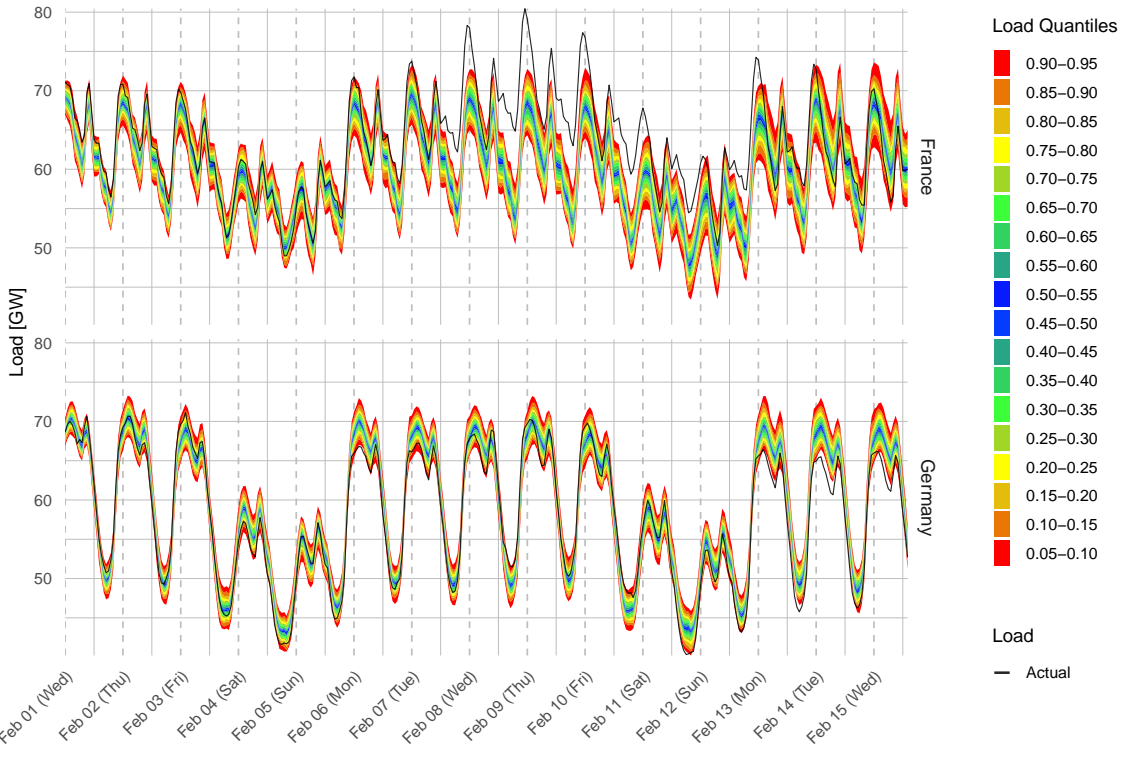


Figure 17: Quantiles of the VETS model (forecasting experiment $N = 50$) in France and Germany forecasting the first two weeks of the one-year forecasting horizon (February 1st, 2023 to February 15th, 2023).

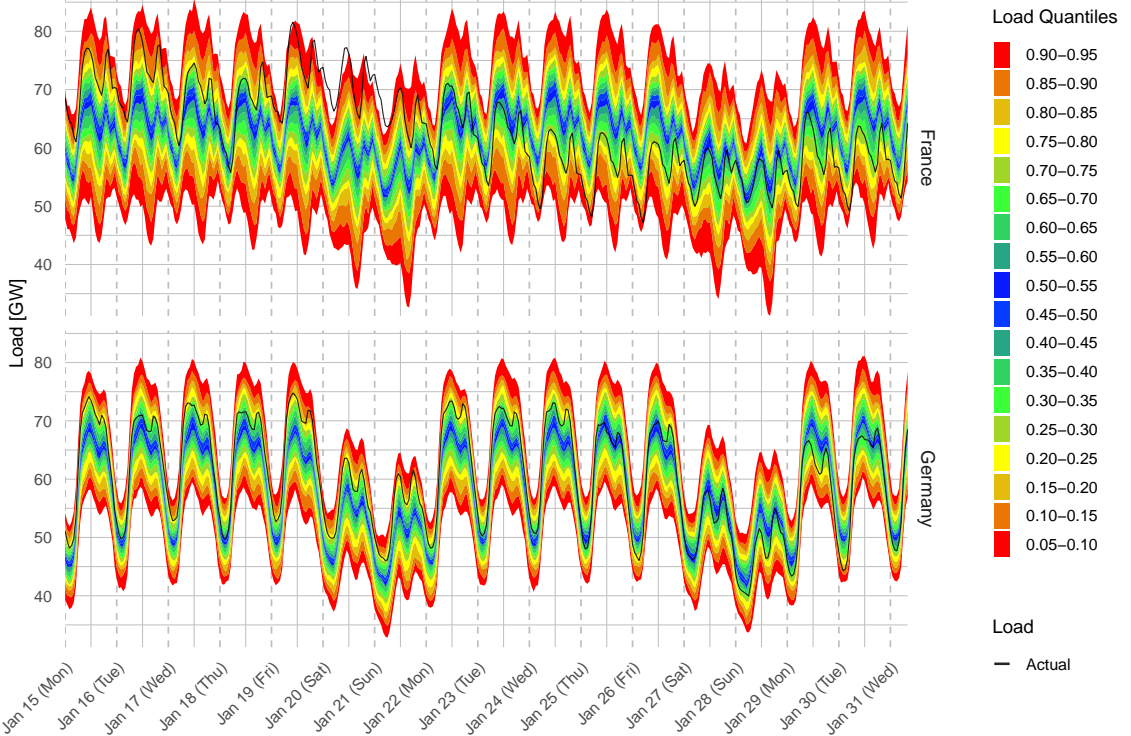


Figure 18: Quantiles of the VETS model (forecasting experiment $N = 50$) in France and Germany forecasting the last two weeks of the one-year forecasting horizon (January 15th, 2024 to January 31st, 2024).

lated as the median of the trajectories summed across all time steps, for both France and Germany over the entire forecasting horizon.

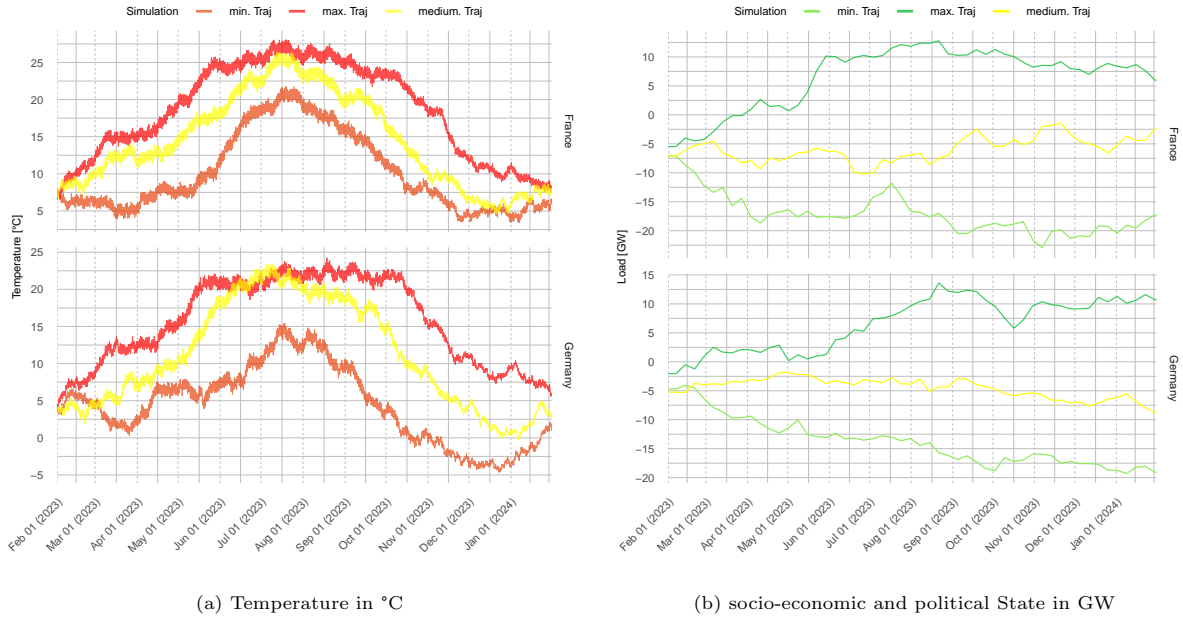


Figure 19: Minimum and maximum trajectory (largest underestimation and overestimation of the 5% and 95% quantiles, respectively, summed over $h = 1, \dots, H$) of the temperature and VETS socio-economic and political state, medium trajectory (median of the summed trajectories over $h = 1, \dots, H$) in France and Germany for the one-year forecasting horizon of forecasting experiment $N = 50$.

For the minimal temperature and maximal socio-economic and political state and autoregressive trajectories, Figures 20-21 visualize the contribution of each deterministic and stochastic modeling input to the load forecast in GW. Additionally, the forecasted load scenario of the probabilistic forecasting model (see Eq. (5)-(6)), resulting from these trajectories, and the point forecasted load (i.e. with zero mean assumption for models in Section 3.2 and no cross-country dependencies, see [Zimmermann & Ziel \(2024\)](#)) are depicted. Both load trajectories were reduced by the estimated intercept.

From these figures, we observe a difference in the deviation between scenario and point forecasts between France and Germany. France exhibits a larger discrepancy (around 20 GW) due to a stronger combined effect from extreme temperature, socio-economic and political scenarios. These risky scenarios contribute roughly 17 GW and 13 GW, respectively, to the probabilistic load in France, in contrast to 6 GW and 10 GW in Germany. For comparison, the corresponding point forecast model explained approximately 1-2 GW in French and German in-sample load by the socio-economic and political state through several years of winter months. In the same period, temperature effects on French load varied between -2 GW up to 20 GW, in uncommonly cold periods, and were mostly negligible for German load, see [Zimmermann & Ziel \(2024\)](#) for details.

Consequently, the temperature effects induced by the chosen extreme scenario in France are realistic real-world events, making them relevant for risk assessment. Furthermore, Figure 19 shows that the difference between the median and minimum temperature trajectory during the Christmas period is around 5°C in France compared to 17°C in Germany. Thus, even though temperature scenarios are less

extreme in France, they already represent around 32% of the French yearly moving average load (between 50-55 GW, see Fig. 2).

The impact of extreme temperature scenarios on French electricity load provides a baseline for scenarios where similar temperature sensitivity is present across many European countries, such as in cases of widespread adoption of electric heating. For instance, one could apply a capacity-scaled temperature effect estimated for France in (5) to other European countries and evaluate the pan-European electricity demand under different temperature scenarios.

A comparison of the VETS to the VAR modeling approach (see Fig. 38-39, Appendix B) under extreme socio-economic and political scenarios reveals lower impacts estimated for the VAR model (approximately 2-10 GW in France, 2-3 GW in Germany). Given that the Christmas holiday period falls near the end of the one-year forecasting horizon (January 31st, 2024 for experiment N=50) and that due to the stationary property of the VAR model state levels converge towards zero, this lower impact is reasonable. Conversely, recall that in the VETS model state levels are continued persistently in the prediction horizon.

The extreme autoregressive scenario has a minimal impact in both countries, contributing between 1 and 5 GW (positive or negative) to the load forecast.

7. Conclusion and Discussion

This paper presents an interpretable cross-country dependent probabilistic mid-term forecasting model for the hourly load that captures, besides all deterministic effects, uncertain temperature, socio-economic and political, and autoregressive effects on load. The model's interpretability allows for clear decomposition of transmission under any given scenario for uncertain load drivers, making it highly suitable for risk assessment. In a scenario analysis, extreme temperatures explained approximately 32% of the French yearly moving average load.

The proposed probabilistic forecasting method may be improved further: Firstly, assuming homoscedasticity of residuals may not be appropriate, in particular, when electricity consumption is becoming more volatile due to widespread electric heating. As Ziel & Liu (2016) argue, variation in load is higher during peak hours and seasons. Thus, in a first approach, heteroscedasticity could be tackled by calculating hour-specific sample covariance matrices. Alternatively, more sophisticated approaches such as GARCH models applied to residuals, as proposed by several methods summarized in Davis et al. (2016), or GAMs modeling time-varying distribution parameters, as proposed in Gioia et al. (2024); Browell & Fasiolo (2021), could be employed.

Secondly, long-term socio-economic and political indicators could be included in the model, as implemented by González Grandón et al. (2024). Examples encompass GDP, population growth, country-specific conflict indices or a COVID-Lockdown dummy, for in-sample handling of the COVID-19 pandemic. By incorporating these exogenous variables, into the VETS model, see Svetunkov (2023) for modeling details, over or underestimation of persistent state forecasts and the consequent error accumulation could be mitigated. Alternatively, they could be incorporated in a regression framework on seasonally aggregated load values as suggested for the long-term trend model in González Grandón et al.

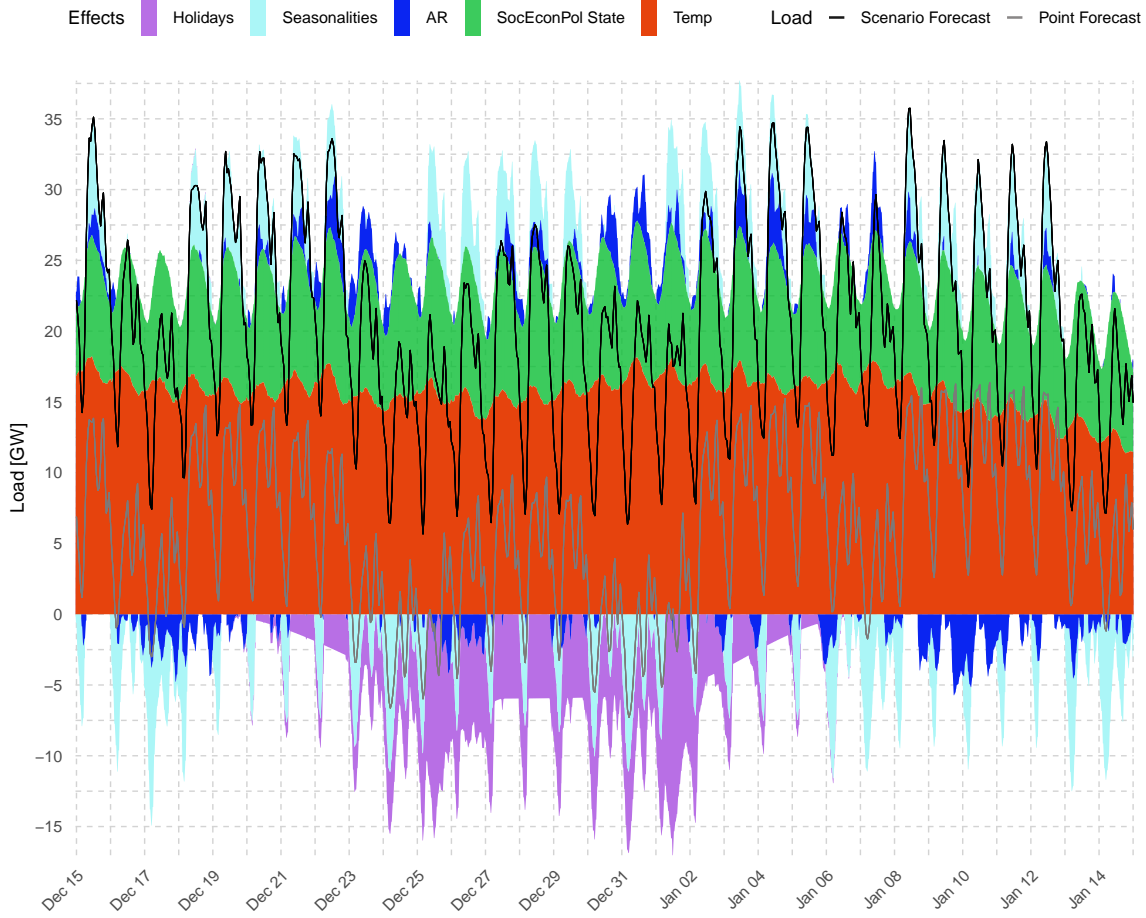


Figure 20: Forecasted load scenario (see (5) - (7)) decomposed in its modeling components for min. temperature, max. socio-economic and political state and max. autoregressive trajectories along with point forecasted load reduced by the estimated intercept for the **VETS** model (forecasting experiment $N = 50$) in France from December 15th, 2023 to January 14th, 2024.

(2024) or our proposed **VAR** and **VECM** models. However, a challenge in using exogenous variables is the need for reliable mid-term forecasts, as emphasized by [González Grandón et al. \(2024\)](#). Moreover, forecasting combinations of models like **VETS** assuming a persistent trend and models like **VAR** assuming a trend converging to zero could be considered for the socio-economic and political state.

Lastly, in anticipation of an energy transition and the increasing dependence of load on weather, which is expected to become more volatile in the long-term due to climate change, see [Mosquera-López et al. \(2024\)](#), one could incorporate a climate trend and a longer historical time horizon in the temperature model to improve risk assessment.

Author Contributions

M. Z.: Conceptualization; methodology; software; validation; formal analysis; investigation; data curation; writing - original draft; writing review and editing; visualization.

F. Z.: Conceptualization; methodology; validation; formal analysis; funding acquisition; resources; writing - review and editing; supervision.

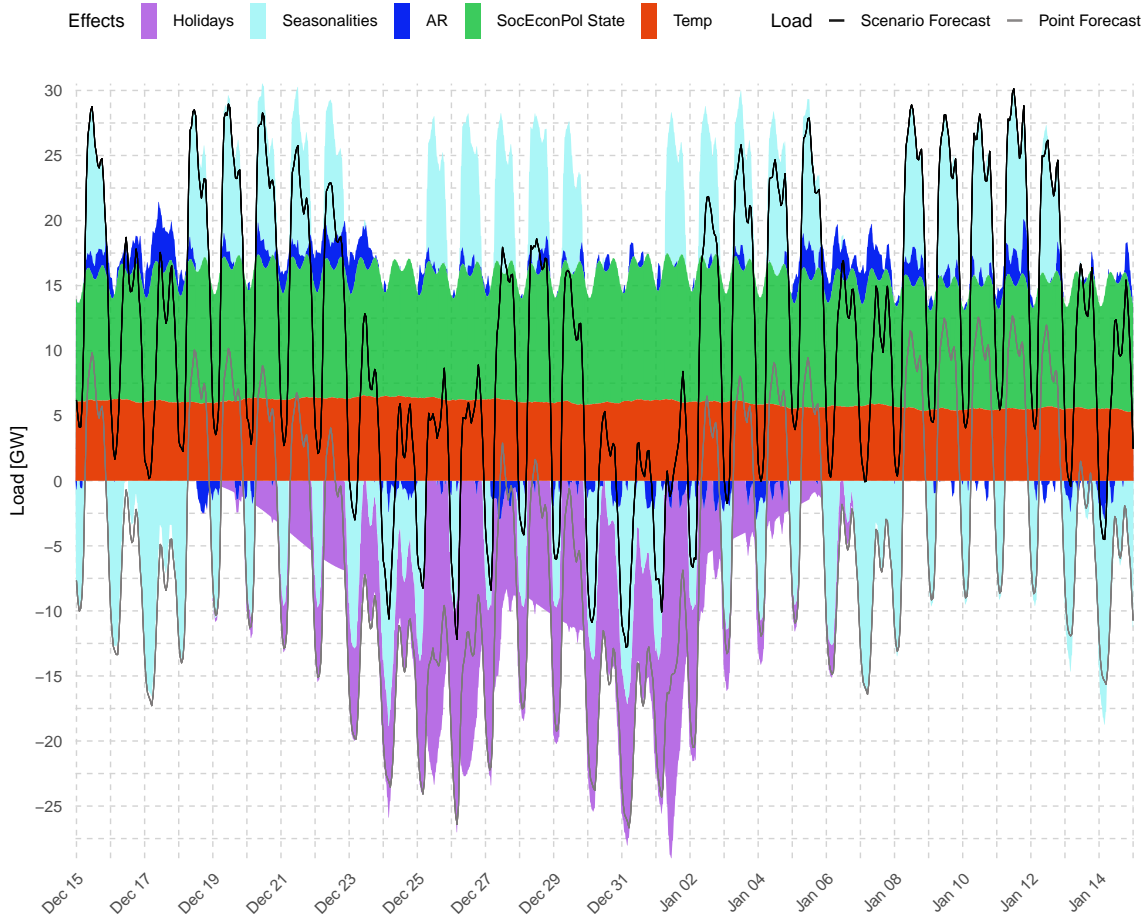


Figure 21: Forecasted load scenario (see (5) - (7)) decomposed in its modeling components for min. temperature, max. socio-economic and political state and max. autoregressive trajectories along with point forecasted load reduced by the estimated intercept for the VETS model (forecasting experiment $N = 50$) in Germany from December 15th, 2023 to January 14th, 2024.

Funding Statement

This research has been funded by the Deutsche Forschungsgemeinschaft (DFG, German Research Foundation) – 505565850.

References

- Agrawal, R. K., Muchahary, F., & Tripathi, M. M. (2018). Long term load forecasting with hourly predictions based on long-short-term-memory networks. In *2018 IEEE Texas Power and Energy Conference (TPEC)* (pp. 1–6). College Station, TX: IEEE. URL: <http://ieeexplore.ieee.org/document/8312088/>. doi:[10.1109/TPEC.2018.8312088](https://doi.org/10.1109/TPEC.2018.8312088).
- Altermatt, P. P., Clausen, J., Brendel, H., Breyer, C., Gerhards, C., Kemfert, C., Weber, U., & Wright, M. (2023). Replacing gas boilers with heat pumps is the fastest way to cut German gas consumption. *Communications Earth & Environment*, 4, 56. URL: <https://www.nature.com/articles/s43247-023-00715-7>. doi:[10.1038/s43247-023-00715-7](https://doi.org/10.1038/s43247-023-00715-7).
- Bashiri Behmiri, N., Fezzi, C., & Ravazzolo, F. (2023). Incorporating air temperature into mid-term electricity load forecasting models using time-series regressions and neural networks. *Energy*, 278, 127831. doi:[10.1016/j.energy.2023.127831](https://doi.org/10.1016/j.energy.2023.127831).

- Baviera, R., & Messuti, G. (2023). Daily middle-term probabilistic forecasting of power consumption in North-East England. *Energy Systems*, . URL: <https://link.springer.com/10.1007/s12667-023-00577-0>. doi:10.1007/s12667-023-00577-0.
- Behm, C., Nolting, L., & Praktiknjo, A. (2020). How to model European electricity load profiles using artificial neural networks. *Applied Energy*, 277, 115564. URL: <https://linkinghub.elsevier.com/retrieve/pii/S030626192031076X>. doi:10.1016/j.apenergy.2020.115564.
- Bessec, M., & Fouquau, J. (2008). The non-linear link between electricity consumption and temperature in Europe: A threshold panel approach. *Energy Economics*, 30, 2705–2721. doi:10.1016/j.eneco.2008.02.003.
- Bogdanov, D., Satymov, R., & Breyer, C. (2024). Impact of temperature dependent coefficient of performance of heat pumps on heating systems in national and regional energy systems modelling. *Applied Energy*, 371, 123647. URL: <https://linkinghub.elsevier.com/retrieve/pii/S0306261924010304>. doi:10.1016/j.apenergy.2024.123647.
- Browell, J., & Fasiolo, M. (2021). Probabilistic Forecasting of Regional Net-Load With Conditional Extremes and Gridded NWP. *IEEE Transactions on Smart Grid*, 12, 5011–5019. URL: <https://ieeexplore.ieee.org/document/9520817/>. doi:10.1109/TSG.2021.3107159.
- Brusaferri, A., Matteucci, M., Spinelli, S., & Vitali, A. (2022). Probabilistic electric load forecasting through Bayesian Mixture Density Networks. *Applied Energy*, 309, 118341. URL: <https://linkinghub.elsevier.com/retrieve/pii/S0306261921015907>. doi:10.1016/j.apenergy.2021.118341.
- Davis, K. O., Hong, T., & Fan, S. (2016). Probabilistic electric load forecasting: A tutorial review. *International Journal of Forecasting*, 32, 914–938. doi:10.1016/j.ijforecast.2015.11.011. MAG ID: 2275088575 S2ID: 154102a5a5e3a96fc37bd5e672137126f323490.
- De Silva, A., Hyndman, R. J., & Snyder, R. (2010). The vector innovations structural time series framework: a simple approach to multivariate forecasting. *Statistical Modelling*, 10, 353–374. URL: <http://journals.sagepub.com/doi/10.1177/1471082X0901000401>. doi:10.1177/1471082X0901000401.
- De Vilmarest, J., Browell, J., Fasiolo, M., Goude, Y., & Wintenberger, O. (2024). Adaptive Probabilistic Forecasting of Electricity (Net-)Load. *IEEE Transactions on Power Systems*, 39, 4154–4163. URL: <https://ieeexplore.ieee.org/document/10234679/>. doi:10.1109/TPWRS.2023.3310280.
- De Vilmarest, J., & Goude, Y. (2022). State-Space Models for Online Post-Covid Electricity Load Forecasting Competition. *IEEE Open Access Journal of Power and Energy*, 9, 192–201. doi:10.1109/OAJPE.2022.3141883.
- Dordonnat, V., Pichavant, A., & Pierrot, A. (2016). GEFCom2014 probabilistic electric load forecasting using time series and semi-parametric regression models. *International Journal of Forecasting*, 32, 1005–1011. doi:10.1016/j.ijforecast.2015.11.010.
- Dudek, G. (2022). A Comprehensive Study of Random Forest for Short-Term Load Forecasting. *Energies*, 15, 7547. URL: <https://www.mdpi.com/1996-1073/15/20/7547>. doi:10.3390/en15207547.
- Fan, S., & Hyndman, R. J. (2012). Short-Term Load Forecasting Based on a Semi-Parametric Additive Model. *IEEE Transactions on Power Systems*, 27, 134–141. doi:10.1109/TPWRS.2011.2162082.
- Gaillard, P., Goude, Y., & Nedellec, R. (2016). Additive models and robust aggregation for GEFCom2014 probabilistic electric load and electricity price forecasting. *International Journal of Forecasting*, 32, 1038–1050. doi:10.1016/j.ijforecast.2015.12.001.
- Gil-Alaña, L., & Robinson, P. (1997). Testing of unit root and other nonstationary hypotheses in macroeconomic time series. *Journal of Econometrics*, 80, 241–268. doi:10.1016/S0304-4076(97)00038-9.
- Gilbert, C., Browell, J., & Stephen, B. (2023). Probabilistic load forecasting for the low voltage network: Forecast fusion and daily peaks. *Sustainable Energy, Grids and Networks*, 34, 100998. URL: <https://linkinghub.elsevier.com/retrieve/pii/S2352467723000061>. doi:10.1016/j.segan.2023.100998.

- Gioia, V., Fasiolo, M., Browell, J., & Bellio, R. (2024). Additive Covariance Matrix Models: Modelling Regional Electricity Net-Demand in Great Britain. URL: <http://arxiv.org/abs/2211.07451>.
- Gneiting, T., & Raftery, A. E. (2007). Strictly Proper Scoring Rules, Prediction, and Estimation. *Journal of the American Statistical Association*, 102, 359–378. URL: <http://www.tandfonline.com/doi/abs/10.1198/016214506000001437>. doi:[10.1198/016214506000001437](https://doi.org/10.1198/016214506000001437).
- González Grandón, T., Schwenzer, J., Steens, T., & Breuing, J. (2024). Electricity demand forecasting with hybrid classical statistical and machine learning algorithms: Case study of Ukraine. *Applied Energy*, 355, 122249. URL: <https://linkinghub.elsevier.com/retrieve/pii/S0306261923016136>. doi:[10.1016/j.apenergy.2023.122249](https://doi.org/10.1016/j.apenergy.2023.122249).
- Goodell, J. W., Gurdiev, C., Paltrinieri, A., & Piserà, S. (2023). Global energy supply risk: Evidence from the reactions of European natural gas futures to Nord Stream announcements. *Energy Economics*, 125, 106838. URL: <https://linkinghub.elsevier.com/retrieve/pii/S0140988323003365>. doi:[10.1016/j.eneco.2023.106838](https://doi.org/10.1016/j.eneco.2023.106838).
- Goude, Y., Nedellec, R., & Kong, N. (2014). Local Short and Middle Term Electricity Load Forecasting With Semi-Parametric Additive Models. *IEEE Transactions on Smart Grid*, 5, 440–446. doi:[10.1109/tsg.2013.2278425](https://doi.org/10.1109/tsg.2013.2278425). MAG ID: 1991414280 S2ID: ebf703bad0082d55fbde21f6ef1dc1ed87e46d58.
- Haben, S., Voss, M., & Holderbaum, W. (2023). *Core concepts and methods in load forecasting: with applications in distribution networks*. Cham: Springer.
- Hager, T. (2024). Nager.Date. URL: <https://github.com/nager/Nager.Date>.
- Harvey, A. C., Trimbur, T. M., & Van Dijk, H. K. (2007). Trends and cycles in economic time series: A Bayesian approach. *Journal of Econometrics*, 140, 618–649. doi:[10.1016/j.jeconom.2006.07.006](https://doi.org/10.1016/j.jeconom.2006.07.006).
- Hendry, D. F., & Juselius, K. (2000). Explaining Cointegration Analysis: Part II. *The Energy Journal*, 22, 75–120. doi:[10.5547/issn0195-6574-ej-vol22-no1-4](https://doi.org/10.5547/issn0195-6574-ej-vol22-no1-4).
- Hong, T., Pinson, P., Fan, S., Zareipour, H., Troccoli, A., & Hyndman, R. J. (2016). Probabilistic energy forecasting: Global Energy Forecasting Competition 2014 and beyond. *International Journal of Forecasting*, 32, 896–913. doi:[10.1016/j.ijforecast.2016.02.001](https://doi.org/10.1016/j.ijforecast.2016.02.001).
- Hong, T., Wilson, J., & Xie, J. (2014). Long Term Probabilistic Load Forecasting and Normalization With Hourly Information. *IEEE Transactions on Smart Grid*, 5, 456–462. doi:[10.1109/TSG.2013.2274373](https://doi.org/10.1109/TSG.2013.2274373).
- Jusélius, K. (2009). *The cointegrated VAR model: methodology and applications*. Advanced texts in econometrics (reprinted ed.). Oxford: Oxford Univ. Press.
- Kalhorri, M. R. N., Emami, I. T., Fallahi, F., & Tabarzadi, M. (2022). A data-driven knowledge-based system with reasoning under uncertain evidence for regional long-term hourly load forecasting. *Applied Energy*, 314, 118975. URL: <https://linkinghub.elsevier.com/retrieve/pii/S0306261922003853>. doi:[10.1016/j.apenergy.2022.118975](https://doi.org/10.1016/j.apenergy.2022.118975).
- Koenker, R., & Bassett, G. (1978). Regression Quantiles. *Econometrica*, 46, 33. URL: <https://www.jstor.org/stable/1913643?origin=crossref>. doi:[10.2307/1913643](https://doi.org/10.2307/1913643).
- Kröger, D., Peper, J., & Rehtanz, C. (2023). Electricity market modeling considering a high penetration of flexible heating systems and electric vehicles. *Applied Energy*, 331, 120406. URL: <https://linkinghub.elsevier.com/retrieve/pii/S0306261922016634>. doi:[10.1016/j.apenergy.2022.120406](https://doi.org/10.1016/j.apenergy.2022.120406).
- Lee, J. D., Sun, D. L., Sun, Y., & Taylor, J. E. (2016). Exact post-selection inference, with application to the lasso. *The Annals of Statistics*, 44. doi:[10.1214/15-AOS1371](https://doi.org/10.1214/15-AOS1371).
- Lepore, A., Palumbo, B., & Poggi, J.-M. (Eds.) (2022). *Interpretability for Industry 4.0: statistical and machine learning approaches*. Cham: Springer. OCLC: 1348479084.

- Li, D., Tan, Y., Zhang, Y., Miao, S., & He, S. (2023). Probabilistic forecasting method for mid-term hourly load time series based on an improved temporal fusion transformer model. *International Journal of Electrical Power & Energy Systems*, 146, 108743. URL: <https://linkinghub.elsevier.com/retrieve/pii/S0142061522007396>. doi:[10.1016/j.ijepes.2022.108743](https://doi.org/10.1016/j.ijepes.2022.108743).
- Lu, C., Liang, J., Jiang, W., Teng, J., & Wu, C. (2023). High-resolution probabilistic load forecasting: A learning ensemble approach. *Journal of the Franklin Institute*, 360, 4272–4296. URL: <https://linkinghub.elsevier.com/retrieve/pii/S0016003223000911>. doi:[10.1016/j.jfranklin.2023.02.010](https://doi.org/10.1016/j.jfranklin.2023.02.010).
- Ludwig, N., Arora, S., & Taylor, J. W. (2023). Probabilistic load forecasting using post-processed weather ensemble predictions. *Journal of the Operational Research Society*, 74, 1008–1020. doi:[10.1080/01605682.2022.2115411](https://doi.org/10.1080/01605682.2022.2115411).
- Meteostat Developers (2024). Meteostat Developers. URL: <https://dev.meteostat.net/>.
- Moral-Carcedo, J., & Pérez-García, J. (2019). Time of day effects of temperature and daylight on short term electricity load. *Energy*, 174, 169–183. URL: <https://linkinghub.elsevier.com/retrieve/pii/S0360544219303573>. doi:[10.1016/j.energy.2019.02.158](https://doi.org/10.1016/j.energy.2019.02.158).
- Mosquera-López, S., Uribe, J. M., & Joaqui-Barandica, O. (2024). Weather conditions, climate change, and the price of electricity. *Energy Economics*, (p. 107789). URL: <https://linkinghub.elsevier.com/retrieve/pii/S0140988324004973>. doi:[10.1016/j.eneco.2024.107789](https://doi.org/10.1016/j.eneco.2024.107789).
- Narayan, P. K., & Liu, R. (2015). A unit root model for trending time-series energy variables. *Energy Economics*, 50, 391–402. URL: <https://linkinghub.elsevier.com/retrieve/pii/S014098831400317X>. doi:[10.1016/j.eneco.2014.11.021](https://doi.org/10.1016/j.eneco.2014.11.021).
- Nelson, C. R., & Plosser, C. R. (1982). Trends and random walks in macroeconomic time series. *Journal of Monetary Economics*, 10, 139–162. URL: <https://linkinghub.elsevier.com/retrieve/pii/0304393282900125>. doi:[10.1016/0304-3932\(82\)90012-5](https://doi.org/10.1016/0304-3932(82)90012-5).
- Perron, P. (1997). Further evidence on breaking trend functions in macroeconomic variables. *Journal of Econometrics*, 80, 355–385. URL: <https://linkinghub.elsevier.com/retrieve/pii/S0304407697000493>. doi:[10.1016/S0304-4076\(97\)00049-3](https://doi.org/10.1016/S0304-4076(97)00049-3).
- Petropoulos, F., Apiletti, D., Assimakopoulos, V., Babai, M. Z., Barrow, D. K., Taieb, S. B., Bergmeir, C., Bessa, R., Bijak, J., Boylan, J. E., Browell, J., Carnevale, C., Castle, J. L., Cirillo, P., Clements, M. P., Cordeiro, C., Oliveira, F. L. C., Baets, S. D., Dokumentov, A., Ellison, J., Fiszeder, P., Franses, P. H., Frazier, D. T., Gilliland, M., Gönül, M. S., Goodwin, P., Grossi, L., Grushka-Cockayne, Y., Guidolin, M., Guidolin, M., Gunter, U., Guo, X., Guseo, R., Harvey, N., Hendry, D. F., Hollyman, R., Januschowski, T., Jeon, J., Jose, V. R. R., Kang, Y., Koehler, A. B., Kolassa, S., Kourentzes, N., Leva, S., Li, F., Litsiou, K., Makridakis, S., Martin, G. M., Martinez, A. B., Meeran, S., Modis, T., Nikolopoulos, K., Önkäl, D., Paccagnini, A., Panagiotelis, A., Panapakidis, I., Pavía, J. M., Pedio, M., Pedregal, D. J., Pinson, P., Ramos, P., Rapach, D. E., Reade, J. J., Rostami-Tabar, B., Rubaszek, M., Sermpinis, G., Shang, H. L., Spiliotis, E., Syntetos, A. A., Talagala, P. D., Talagala, T. S., Tashman, L., Thomakos, D., Thorarinsdottir, T., Todini, E., Arenas, J. R. T., Wang, X., Winkler, R. L., Yusupova, A., & Ziel, F. (2022). Forecasting: theory and practice. *International Journal of Forecasting*, 38, 705–871. URL: <https://www.sciencedirect.com/science/article/pii/S0169207021001758>. doi:<https://doi.org/10.1016/j.ijforecast.2021.11.001>.
- Pierrot, A., & Goude, Y. (2011). Short-Term Electricity Load Forecasting With Generalized Additive Models. *2011*, .
- Roth, A. (2023). Power sector impacts of a simultaneous European heat pump rollout. URL: <http://arxiv.org/abs/2312.06589> arXiv:2312.06589 [econ, q-fin].
- Roth, A., Kirchem, D., Gaete-Morales, C., & Schill, W.-P. (2023). Flexible heat pumps: must-have or nice to have in a power sector with renewables? URL: <http://arxiv.org/abs/2307.12918> arXiv:2307.12918 [econ, q-fin].

- Ruhnau, O., Lundström, L., Dürr, L., & Hunecke, F. (2023). Empirical weather dependency of heat pump load: Disentangling the effects of heat demand and efficiency. In *2023 19th International Conference on the European Energy Market (EEM)* (pp. 1–5). Lappeenranta, Finland: IEEE. URL: <https://ieeexplore.ieee.org/document/10161914/>. doi:[10.1109/EEM58374.2023.10161914](https://doi.org/10.1109/EEM58374.2023.10161914).
- Schneider, N., & Strielkowski, W. (2023). Modelling the unit root properties of electricity data—A general note on time-domain applications. *Physica A: Statistical Mechanics and its Applications*, *618*, 128685. URL: <https://linkinghub.elsevier.com/retrieve/pii/S0378437123002406>. doi:[10.1016/j.physa.2023.128685](https://doi.org/10.1016/j.physa.2023.128685).
- Shen, Y., Sun, X., Ji, Q., & Zhang, D. (2023). Climate events matter in the global natural gas market. *Energy Economics*, *125*, 106887. URL: <https://linkinghub.elsevier.com/retrieve/pii/S0140988323003857>. doi:[10.1016/j.eneco.2023.106887](https://doi.org/10.1016/j.eneco.2023.106887).
- Smyth, R. (2013). Are fluctuations in energy variables permanent or transitory? A survey of the literature on the integration properties of energy consumption and production. *Applied Energy*, *104*, 371–378. URL: <https://linkinghub.elsevier.com/retrieve/pii/S030626191200801X>. doi:[10.1016/j.apenergy.2012.10.069](https://doi.org/10.1016/j.apenergy.2012.10.069).
- Staffell, I., & Pfenninger, S. (2018). The increasing impact of weather on electricity supply and demand. *Energy*, *145*, 65–78. URL: <https://linkinghub.elsevier.com/retrieve/pii/S0360544217320844>. doi:[10.1016/j.energy.2017.12.051](https://doi.org/10.1016/j.energy.2017.12.051).
- Svetunkov, I. (2023). *Forecasting and Analytics with the Augmented Dynamic Adaptive Model (ADAM)*. (1st ed.). Boca Raton: Chapman and Hall/CRC. URL: <https://www.taylorfrancis.com/books/9781003452652>. doi:[10.1201/9781003452652](https://doi.org/10.1201/9781003452652).
- Svetunkov, I., Chen, H., & Boylan, J. E. (2023). A new taxonomy for vector exponential smoothing and its application to seasonal time series. *European Journal of Operational Research*, *304*, 964–980. URL: <https://linkinghub.elsevier.com/retrieve/pii/S037722172200354X>. doi:[10.1016/j.ejor.2022.04.040](https://doi.org/10.1016/j.ejor.2022.04.040).
- Verwiebe, P. A., Seim, S., Burges, S., Schulz, L., & Müller-Kirchenbauer, J. (2021). Modeling Energy Demand—A Systematic Literature Review. *Energies*, *14*, 7859. doi:[10.3390/en14237859](https://doi.org/10.3390/en14237859).
- Wang, J., Wang, K., Li, Z., Lu, H., Jiang, H., & Xing, Q. (2024). A Multitask Integrated Deep-Learning Probabilistic Prediction for Load Forecasting. *IEEE Transactions on Power Systems*, *39*, 1240–1250. URL: <https://ieeexplore.ieee.org/document/10070851/>. doi:[10.1109/TPWRS.2023.3257353](https://doi.org/10.1109/TPWRS.2023.3257353).
- Watson, S., Crawley, J., Lomas, K., & Buswell, R. (2023). Predicting future GB heat pump electricity demand. *Energy and Buildings*, *286*, 112917. URL: <https://linkinghub.elsevier.com/retrieve/pii/S0378778823001470>. doi:[10.1016/j.enbuild.2023.112917](https://doi.org/10.1016/j.enbuild.2023.112917).
- Wood, S. N. (2006). *Generalized additive models: an introduction with R*. Texts in statistical science. Boca Raton, FL: Chapman & Hall/CRC.
- Xie, J., Chen, Y., Davis, K. O., Hong, T., & Laing, T. D. (2018). Relative Humidity for Load Forecasting Models. *IEEE Transactions on Smart Grid*, *9*, 191–198. doi:[10.1109/tsg.2016.2547964](https://doi.org/10.1109/tsg.2016.2547964).
- Yang, Y., Xing, Q., Wang, K., Li, C., Wang, J., & Huang, X. (2024). A novel combined probabilistic load forecasting system integrating hybrid quantile regression and knee improved multi-objective optimization strategy. *Applied Energy*, *356*, 122341. URL: <https://linkinghub.elsevier.com/retrieve/pii/S0306261923017051>. doi:[10.1016/j.apenergy.2023.122341](https://doi.org/10.1016/j.apenergy.2023.122341).
- Zhang, S., Liu, J., & Wang, J. (2023). High-Resolution Load Forecasting on Multiple Time Scales Using Long Short-Term Memory and Support Vector Machine. *Energies*, *16*, 1806. URL: <https://www.mdpi.com/1996-1073/16/4/1806>. doi:[10.3390/en16041806](https://doi.org/10.3390/en16041806).
- Ziel, F. (2018). Modeling public holidays in load forecasting: a German case study. *Modern power systems*, *6*, 191–207. doi:[10.1007/s40565-018-0385-5](https://doi.org/10.1007/s40565-018-0385-5).

Ziel, F. (2019). Quantile regression for the qualifying match of GEFCom2017 probabilistic load forecasting. *International Journal of Forecasting*, 35, 1400–1408. doi:[10.1016/j.ijforecast.2018.07.004](https://doi.org/10.1016/j.ijforecast.2018.07.004).

Ziel, F., & Liu, B. (2016). Lasso estimation for GEFCom2014 probabilistic electric load forecasting. *International Journal of Forecasting*, 32, 1029–1037. doi:[10.1016/j.ijforecast.2016.01.001](https://doi.org/10.1016/j.ijforecast.2016.01.001).

Zimmermann, M., & Ziel, F. (2024). Efficient Mid-Term Forecasting of Hourly Electricity Load Using Generalized Additive Models. URL: <https://www.ssrn.com/abstract=4823013>. doi:[10.2139/ssrn.4823013](https://doi.org/10.2139/ssrn.4823013).

Appendices

A. Correlation Tables

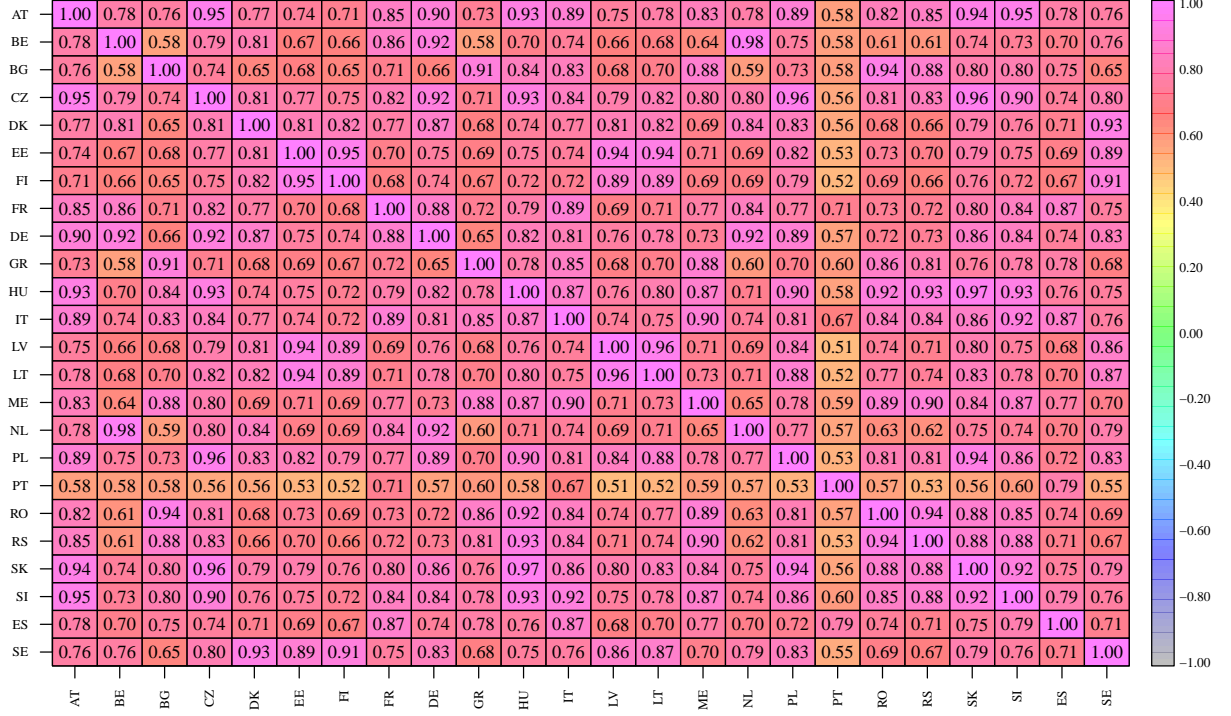


Figure 22: The in-sample correlation matrix $\widehat{\text{Corr}}(\epsilon_t^{\text{Temp}})$ for t from February 6th, 2019 to February 1st, 2023 and smoothing parameter $\alpha = 1/(14 \times 24)$.

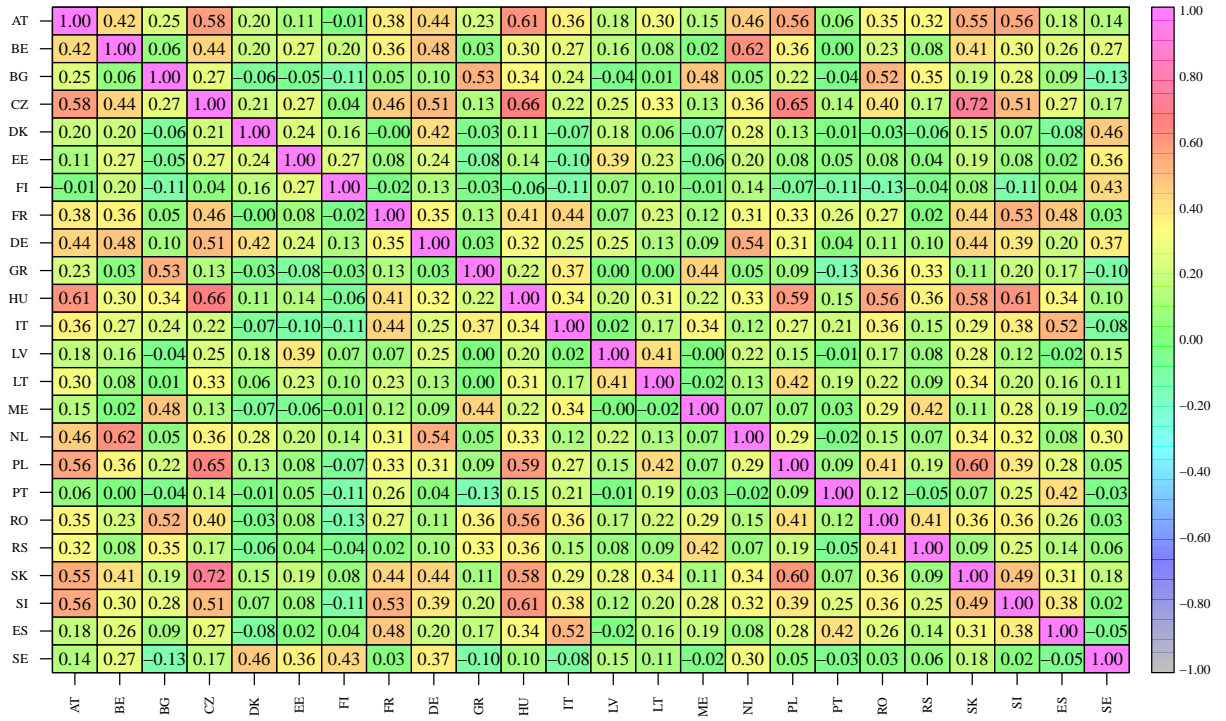
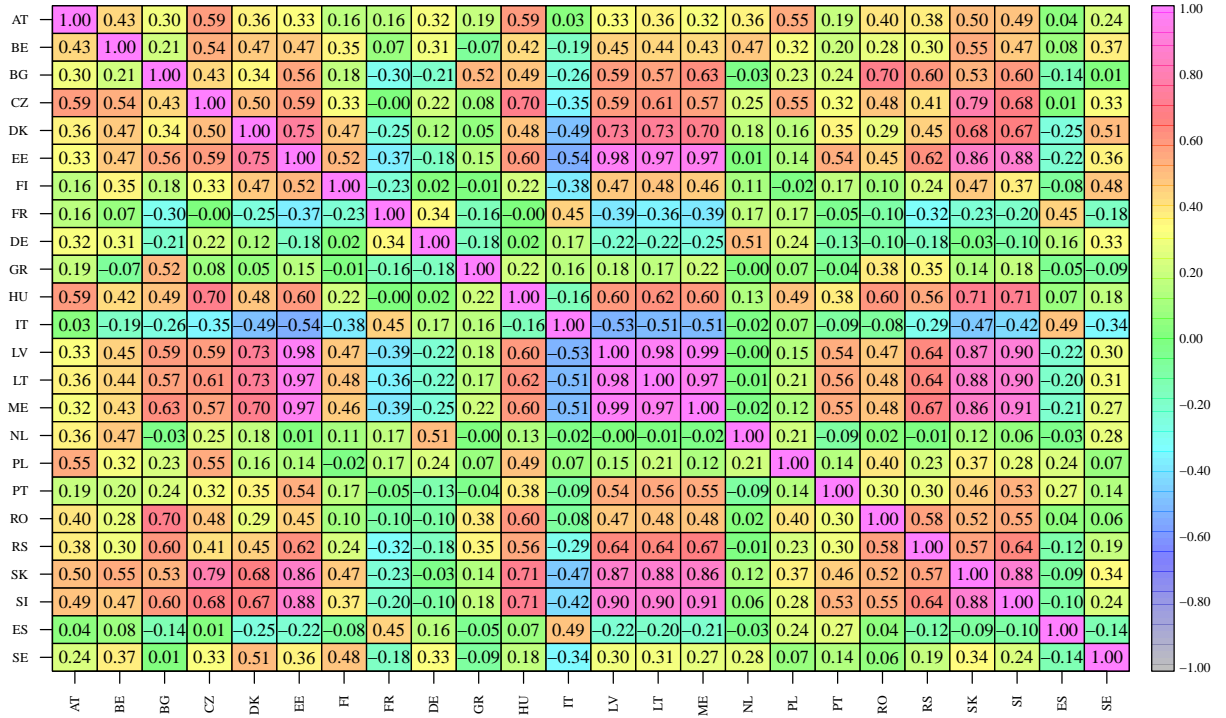


Figure 23: The in-sample correlation matrix $\widehat{\text{Corr}}(\epsilon_{\tau=1,\dots,T/(7 \times 24)}^{\text{VAR}})$ for τ from February 6th, 2019 to February 1st, 2023.



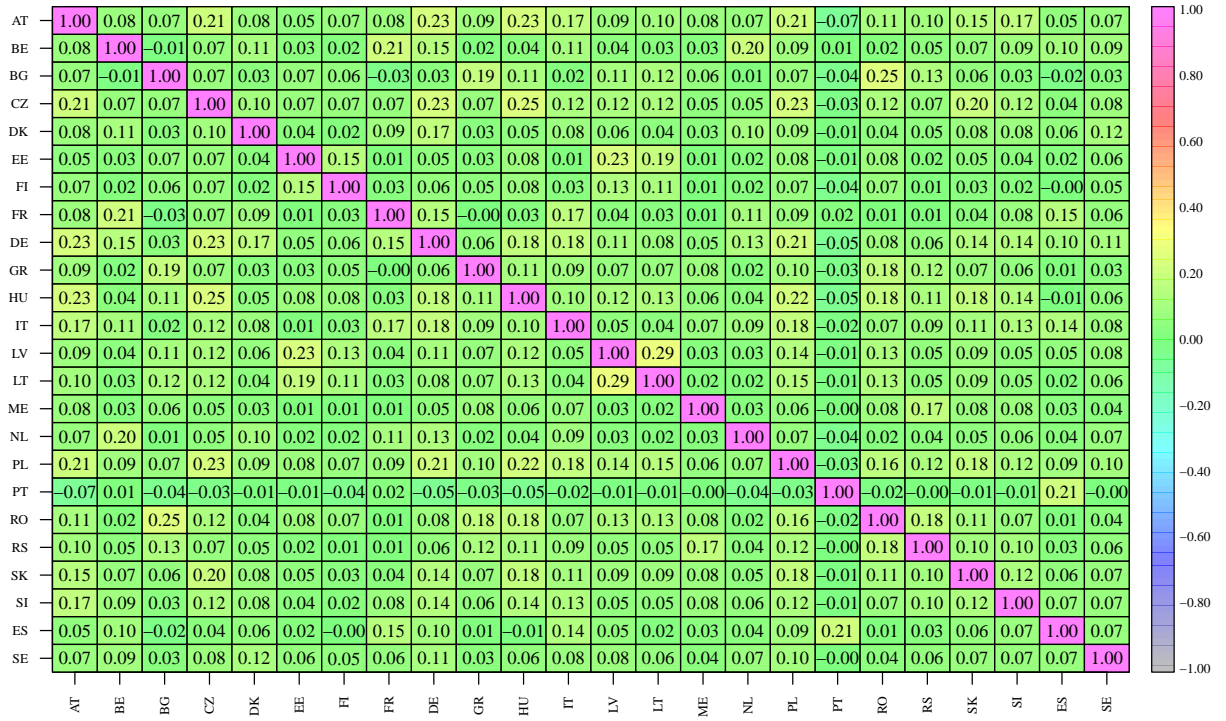
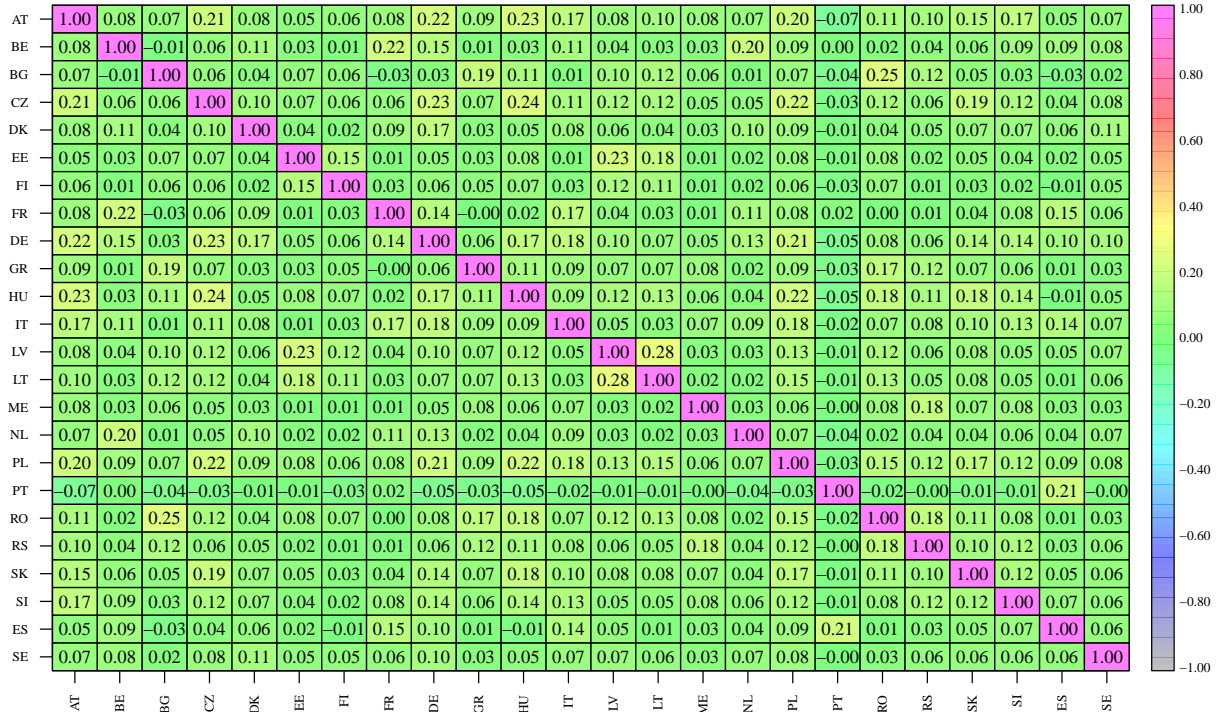


Figure 25: The in-sample correlation matrix $\widehat{\text{Corr}}(\epsilon_t^{\text{AR}})$ for t from February 6th, 2019 to February 1st, 2023 and the VECM model for the socioeconomic state.



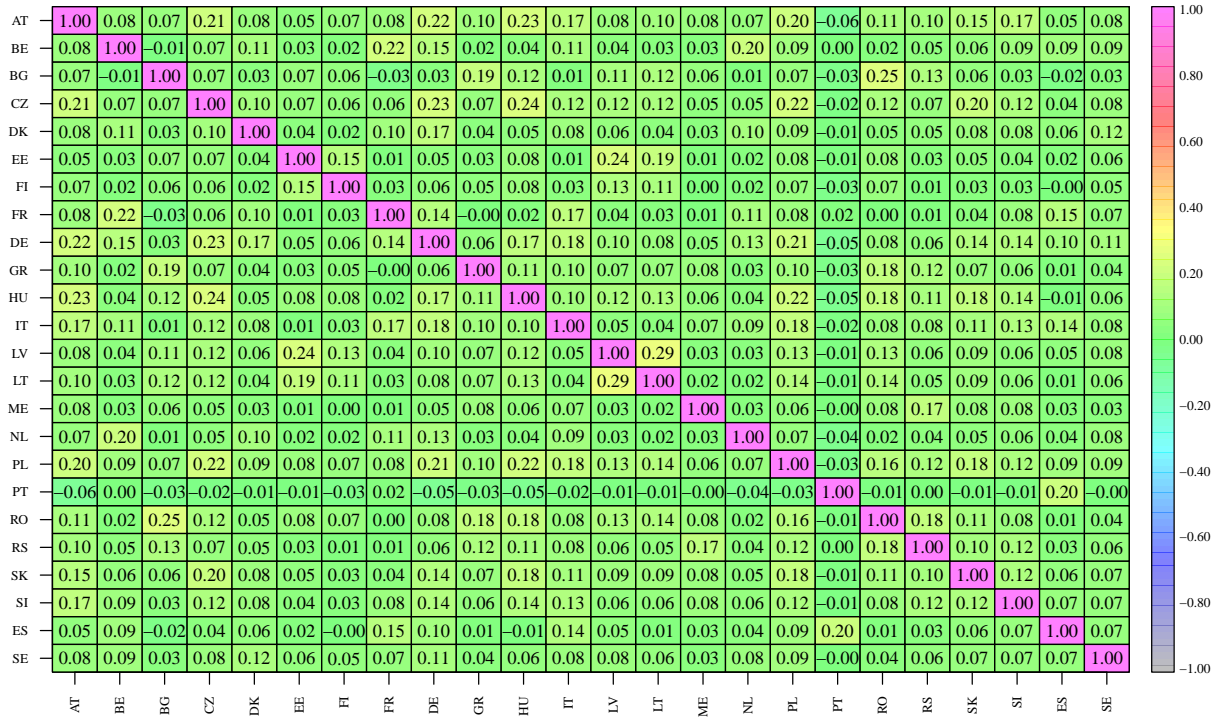
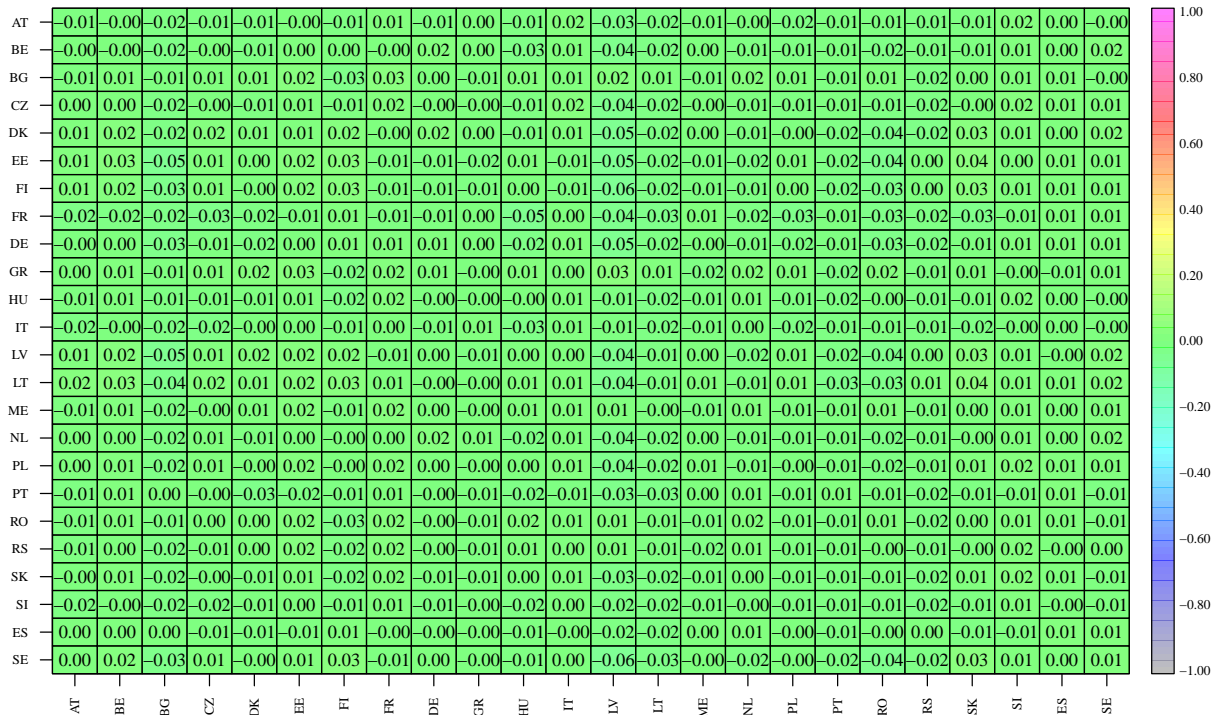


Figure 27: The in-sample correlation matrix $\widehat{\text{Corr}}(\epsilon_t^{\text{AR}})$ for t from February 6th, 2019 to February 1st, 2023 and the VETS model for the socio-economic and political state.



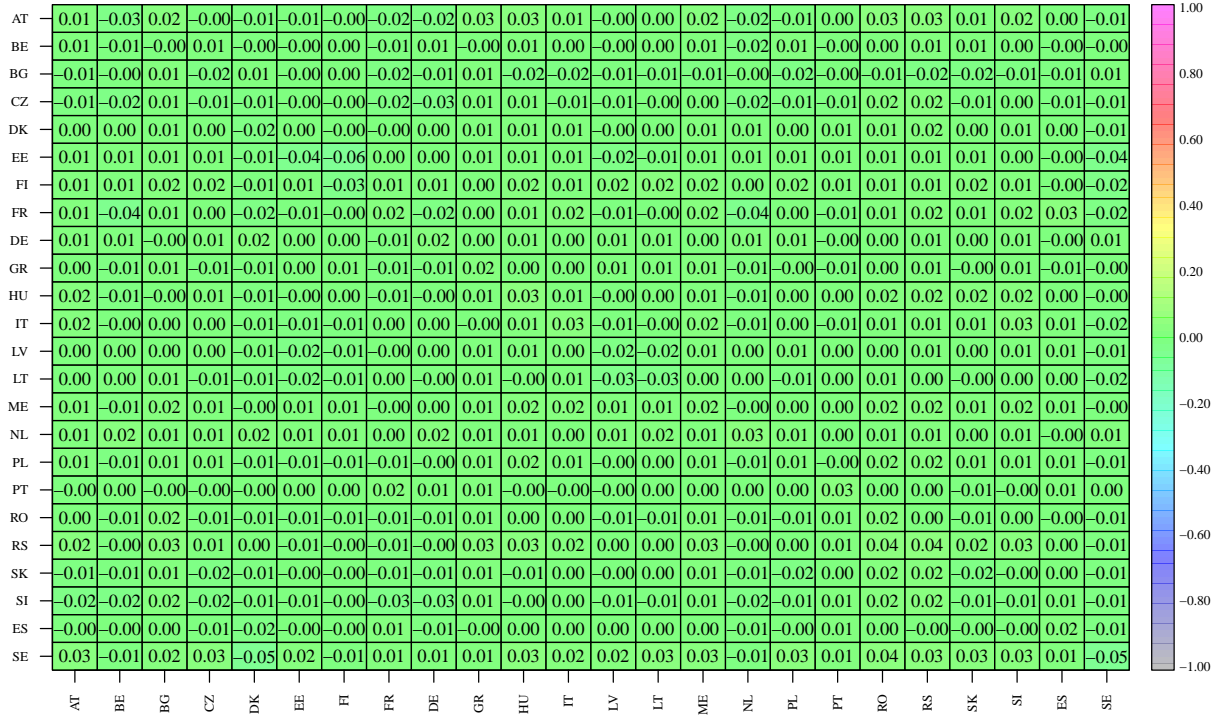


Figure 29: The in-sample correlation matrix $\widehat{\text{Corr}}(\epsilon_{t=1,\dots,T}^{\text{Temp}}, \epsilon_{t=1,\dots,T}^{\text{AR}})$ for t from February 6th, 2019 to February 1st, 2023, $\alpha = 1/24$ and VECM model for the socio-economic and political state.

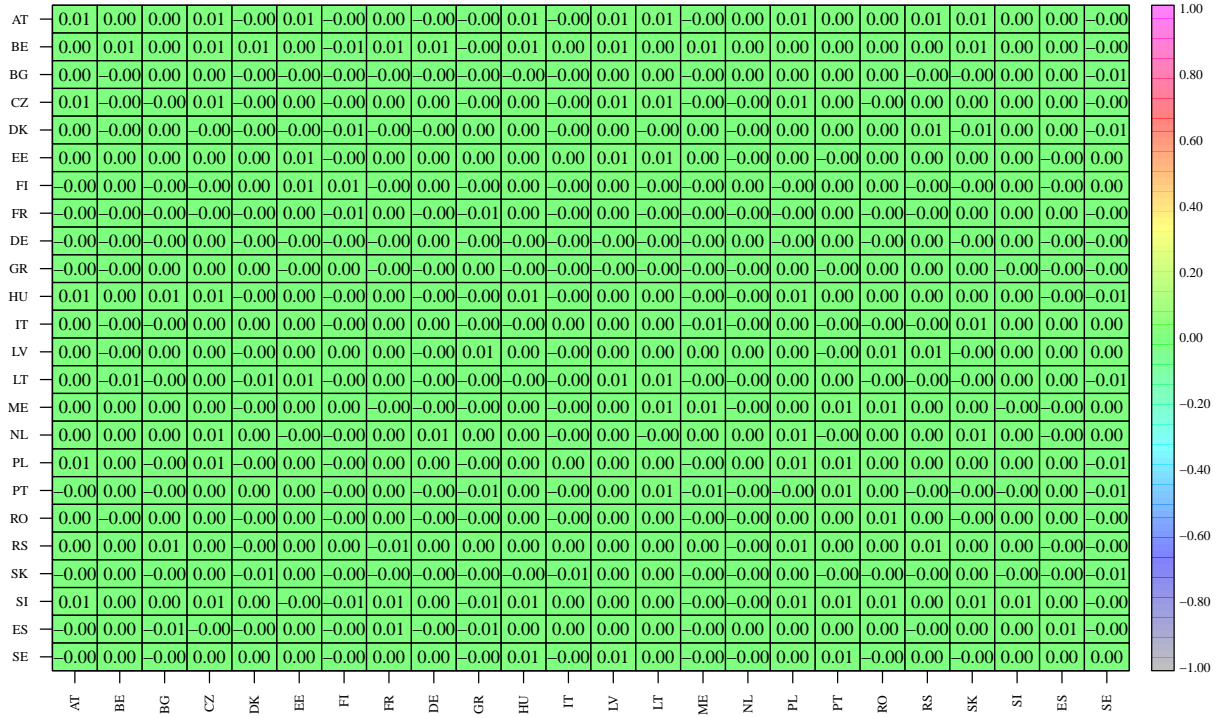


Figure 30: The in-sample correlation matrix $\widehat{\text{Corr}}(\epsilon_{t=1,\dots,T}^{\text{VECM}}, \epsilon_{t=1,\dots,T}^{\text{AR}})$ for t from February 6th, 2019 to February 1st, 2023 and VECM model for the socio-economic and political state.

B. Figures

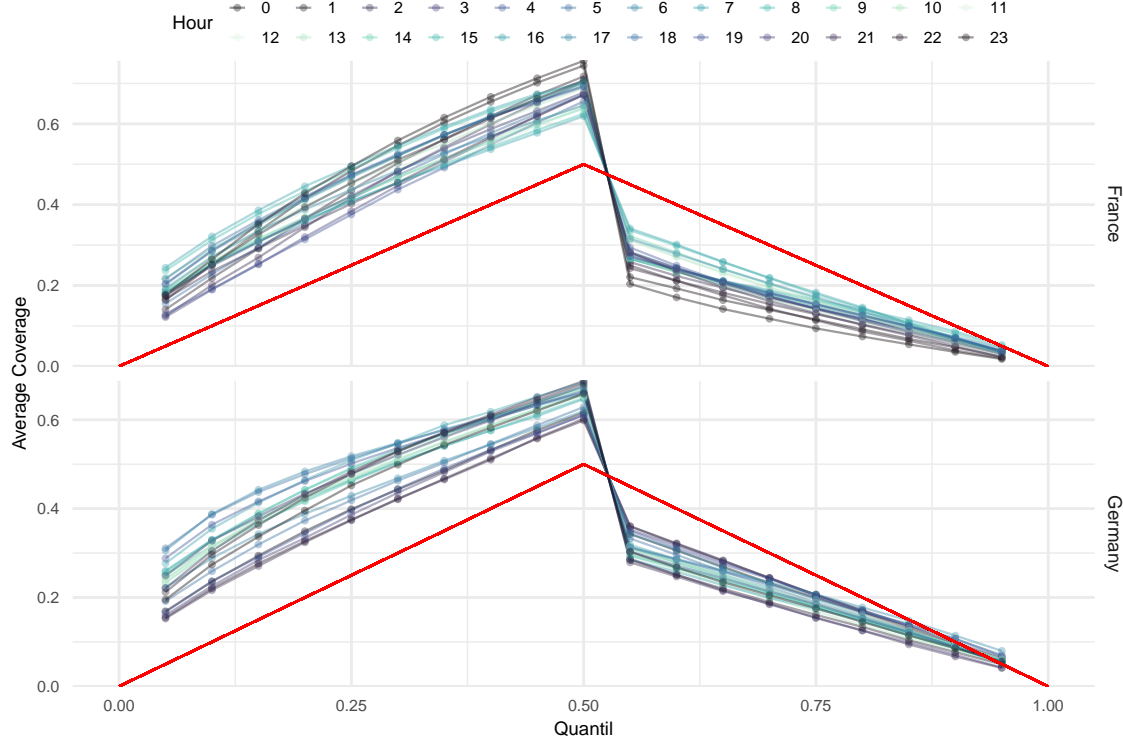


Figure 31: The frequency of underestimations ($q \leq 0.5$) and overestimation ($q > 0.5$) for quantiles $q = 1\%, \dots, 99\%$ of [VECM](#) in $N = 50$ forecasting experiments averaged for each hour of the day for France and Germany.

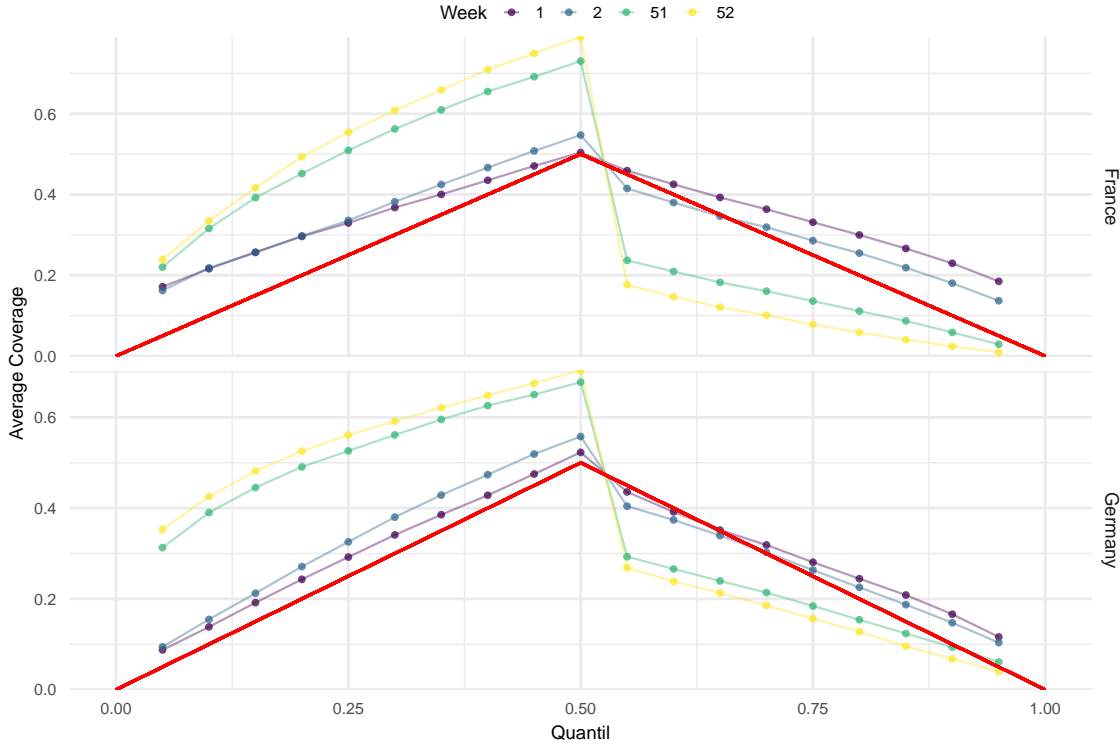


Figure 32: The frequency of underestimations ($q \leq 0.5$) and overestimation ($q > 0.5$) for quantiles $q = 5\%, \dots, 95\%$ of VECM in $N = 50$ forecasting experiments averaged for the first and last two weeks in the forecasting horizon for France and Germany.

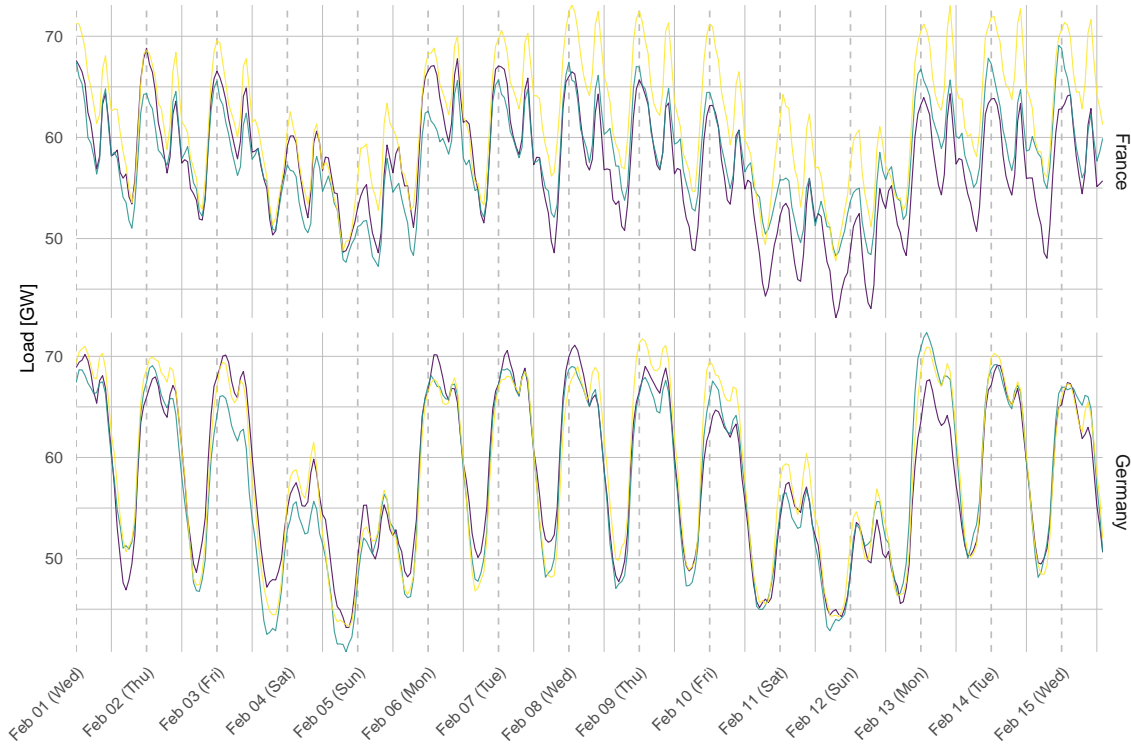


Figure 33: Three sampled load trajectories for the VETS model (forecasting experiment $N = 50$) in France and Germany forecasting the first two weeks of the one-year forecasting horizon (February 1st, 2023 to February 15th, 2023).

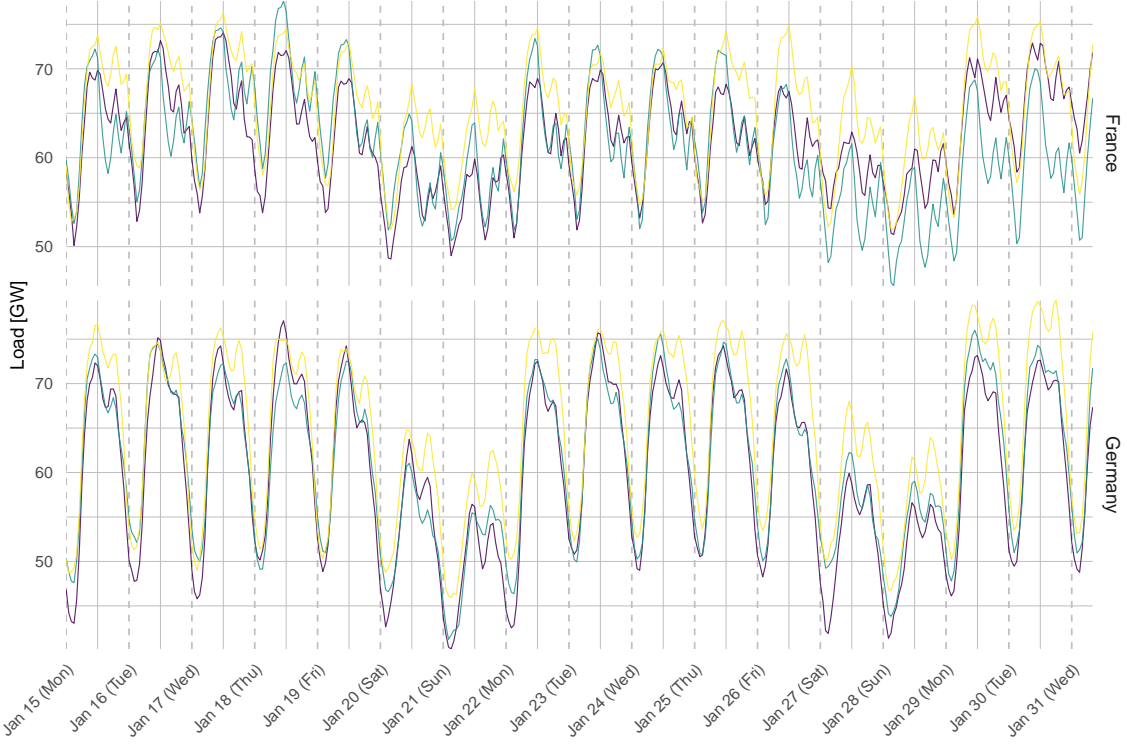


Figure 34: Three sampled load trajectories from the **VAR** model (forecasting experiment $N = 50$) in France and Germany forecasting the last two weeks of the one-year forecasting horizon (January 15th, 2024 to January 31st, 2024).

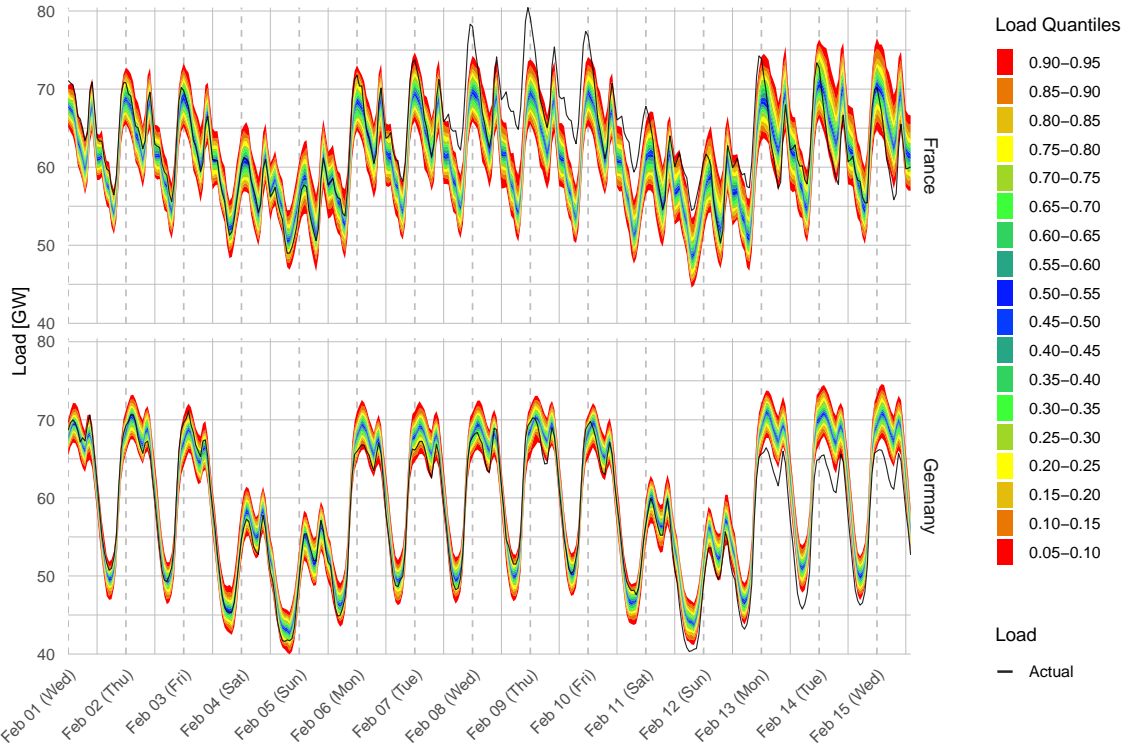


Figure 35: Quantiles of the **VAR** model (forecasting experiment $N = 50$) in France and Germany forecasting the first two weeks of the one-year forecasting horizon (February 1st, 2023 to February 15th, 2023).

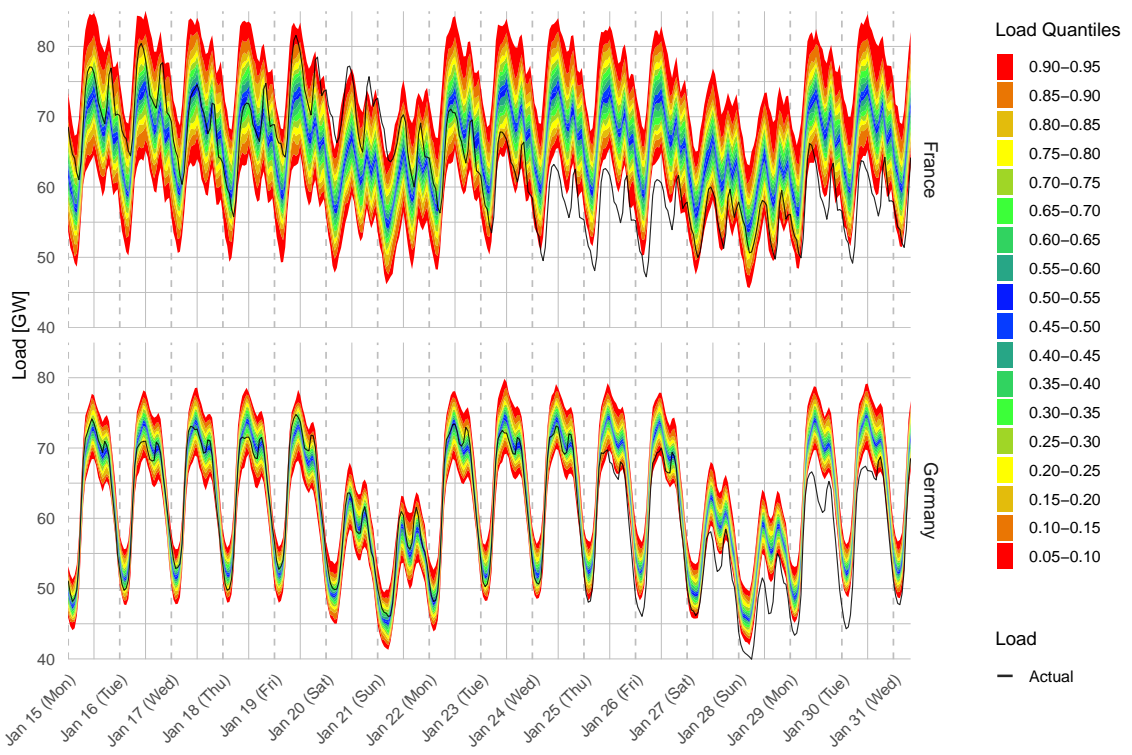


Figure 36: Quantiles of the [VAR](#) model (forecasting experiment $N = 50$) in France and Germany forecasting the last two weeks of the one-year forecasting horizon (January 15th, 2024 to January 31st, 2024).



Figure 37: Minimum and maximum socioeconomic state trajectories (largest underestimation and overestimation of the 5% and 95% quantiles, respectively, summed over $h = 1, \dots, H$) for VAR, medium trajectory (median of the summed trajectories over $h = 1, \dots, H$) in France and Germany for the one-year forecasting horizon of forecasting experiment $N = 50$.

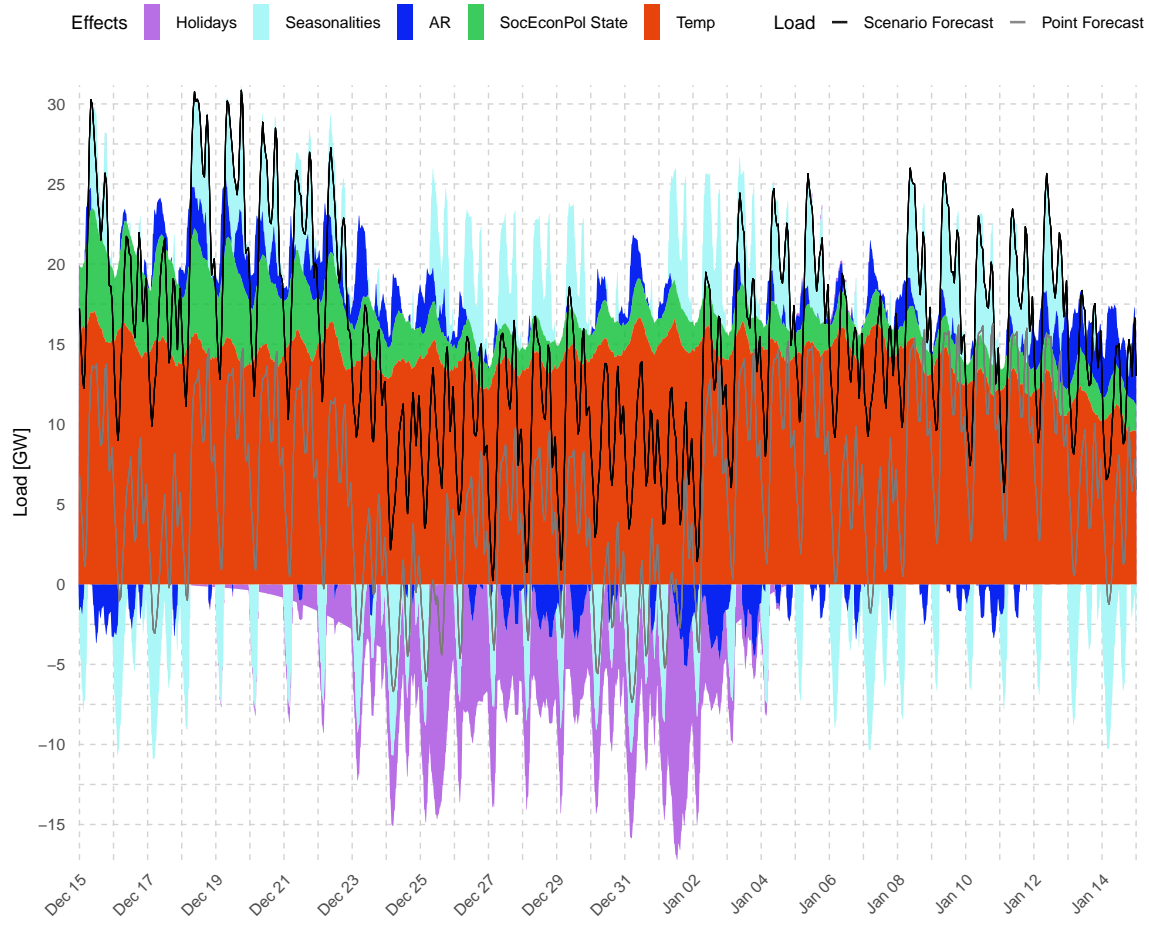


Figure 38: Forecasted load scenario (see (5) - (7)) decomposed in its modeling components for min. temperature, max. socioeconomic state and max. autoregressive trajectories along with point forecasted load reduced by the estimated intercept for the VAR model (forecasting experiment $N = 50$) in France from December 15th, 2023 to January 14th, 2024.

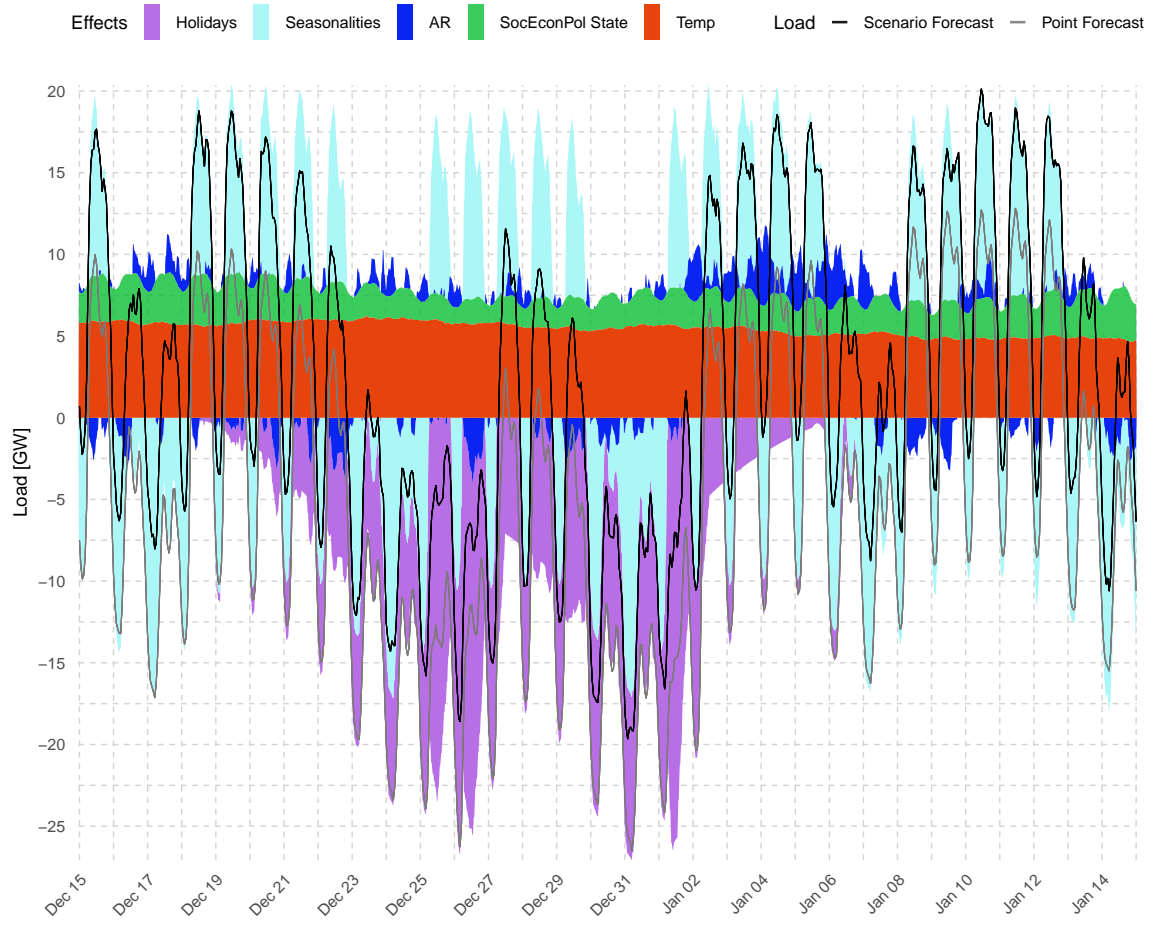


Figure 39: Forecasted load scenario (see (5) - (7)) decomposed in its modeling components for min. temperature, max. socioeconomic state and max. autoregressive trajectories along with point forecasted load reduced by the estimated intercept for the **VAR** model (forecasting experiment $N = 50$) in Germany from December 15th, 2023 to January 14th, 2024.